공학박사 학위논문

소듐-공기 배터리 방전산화물 생성 및 충방전 메커니즘 연구

Fundamental Study on Reaction Mechanism in Rechargeable Na-Air Batteries

2015 년 12 월

서울대학교 대학원

재료공학부

김 진 수

소듐–공기 배터리 방전산화물 생성 및 충방전 메커니즘 연구

지도 교수 강 기 석

이 논문을 공학박사 학위논문으로 제출함

2015 년 10 월

서울대학교 대학원

재료공학부

김 진 수

김진수의 공학박사 학위논문을 인준함

2015 년 12 월

위 원 장 남 기 태 (인)

부위원장 강 기 석 (인)

위 원 이 규 태 (인)

위 원 류 경 한 (인)

위 원 이 윤 정 (인)

Abstract

Recently, metal–air batteries, such as lithium–air and zinc–air systems, have been studied extensively as potential candidates for ultra–high energy density storage devices because of their exceptionally high capacities. Na–O_2 batteries have been regarded as the most promising candidates because of their lower charge overpotential compared with that of the Li–O_2 system, regarding it is abundant and inexpensive. However, conflicting observations with several different discharge products have inhibited the understanding of the precise reactions in the battery.

Firstly in Chapter 2, two types of sodium–oxygen batteries were introduced and studied, i.e., with carbonate and non–carbonate electrolytes. Both types could deliver specific capacities (2800 and 6000 mAh/g) comparable to that of lithium–oxygen batteries but with slightly lower discharge voltages (2.3 V and 2.0 V). The reaction mechanisms of sodium–oxygen batteries in carbonate and non–carbonate electrolytes were investigated and compared with those of lithium–oxygen batteries.

In Chapter 3, we demonstrate that the competition between the electrochemical and chemical reactions in $Na–O_2$ batteries leads to the dissolution and ionization of NaO_2, liberating O_2^- and triggering the formation of $Na_2O_2·2H_2O$. Upon the formation of phases other than NaO_2, the charge overpotential of $Na–O_2$ cells significantly increases. This report is the first verification addressing the origin of the different discharge products and conflicting overpotentials observed in $Na–O_2$ systems. Our proposed model provides guidelines to help direct the reactions in $Na–O_2$ batteries to achieve high efficiency and rechargeability.

Keywords : Energy storage, $Na–O_2$ battery, NaO_2, $Na_2O_2·2H_2O$, Discharge product, Reaction mechanism

Student Number : 2011–30184

Table of Contents

List of Figures

List of Tables

Chapter 1. General Introduction

1.1 Preface

1.1.1 Geopolitical / Ecological Background

Since this century, the global community has been faced the critical situations for the existence of this civilization. The main crisis is come from the unstable supply of energies to sustain the modern society. This systematic world has been grown with the massive consumption of fossil fuels such as petroleum oil, gas and coal.[2] Those have been the essential for the most of power plants, factories and transportations. However, these resources are locally distributed to a few countries, so it has been weaponized to protect their rights and interests. This inhomogeneous accessibility reduced the utilization of the resources in the political and economic point of view.

Nevertheless to consider the geopolitical properties of fossil fuels, it is also issued for those resources to contaminate the natural environment.[2] This class of fuels should be combusted to produce the energy and this process must accompany the emission of various kinds of pollutants such as some exhausted fumes and fine dust. Among them, green–house gases like carbon

dioxide (CO_2) primarily triggered the climate change which means the global warming.[2] Continuous emission of such gases for several decades forced the temperature of the earth to keep rising gradually.[2] In consequence, many nations have been suffered for the unexpected irresistible natural disasters.

To reduce the use of fossil fuel, many countries have tried to promote the utilizations of renewable energies such as solar, wind, geothermal and hydropower energies. These resources are extremely clean, sustainable and ubiquitous in some specific conditions. Thus, it is highly recommended to be used despite of their unsolved technical problems compared to the fossil fuels.

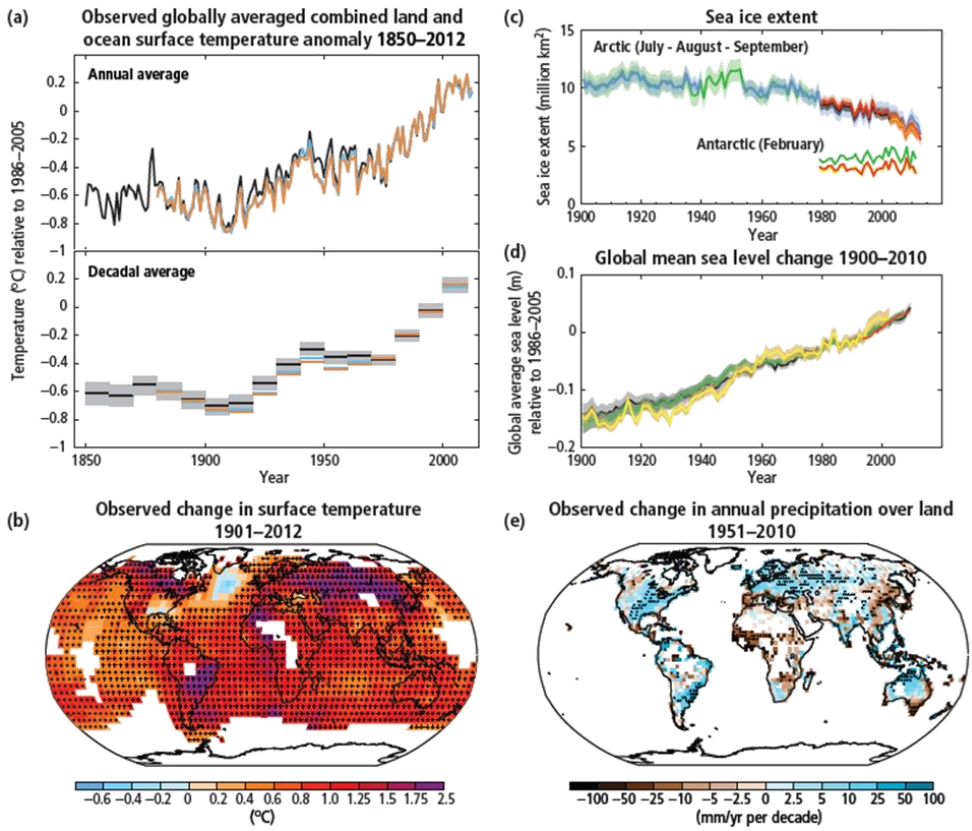

Figure 1–1. Multiple observed indicators of a changing global climate system. IPCC, 2014: *Climate Change 2014: Synthesis Report. Contribution of Working Groups I, II and III to the Fifth Assessment Report of the Intergovernmental Panel on Climate Change* [Core Writing Team, R.K. Pachauri and L.A. Meyer (eds.)]. IPCC, Geneva, Switzerland, 151 pp.[2]

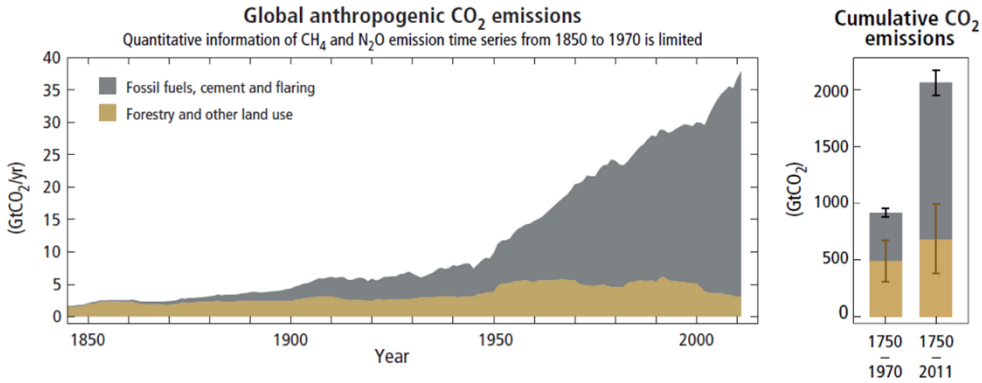

Figure 1–2. Annual global anthropogenic carbon dioxide (CO_2) emissions (gigatonne of CO_2–equivalent per year, $GtCO_2$/yr) from fossil fuel combustion, cement production and flaring, and forestry and other land use (FOLU), 1750~2011. IPCC, 2014: *Climate Change 2014: Synthesis Report. Contribution of Working Groups I, II and III to the Fifth Assessment Report of the Intergovernmental Panel on Climate Change* [Core Writing Team, R.K. Pachauri and L.A. Meyer (eds.)]. IPCC, Geneva, Switzerland, 151 pp.[2]

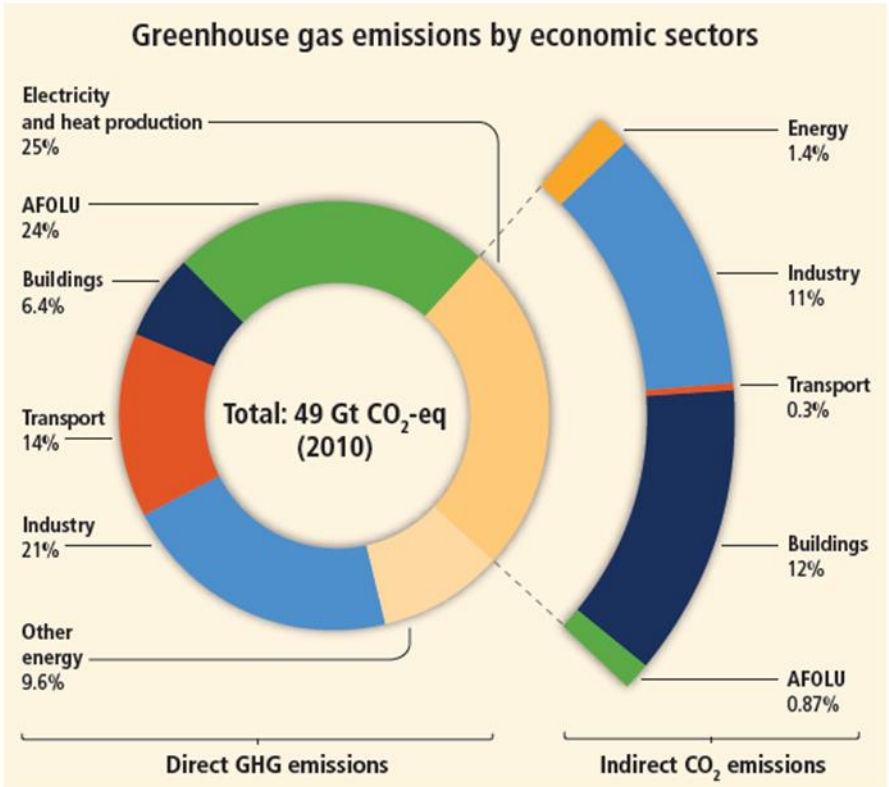

Figure 1–3. Total anthropogenic greenhouse gas (GHG) emissions (gigatonne of CO_2–equivalent per year, $GtCO_2$–eq/yr) from economic sectors in 2010. IPCC, 2014: *Climate Change 2014: Synthesis Report. Contribution of Working Groups I, II and III to the Fifth Assessment Report of the Intergovernmental Panel on Climate Change* [Core Writing Team, R.K. Pachauri and L.A. Meyer (eds.)]. IPCC, Geneva, Switzerland, 151 pp.[2]

1.1.2 Industrial / Economic Background

Although the type of natural resources are quite different, the efforts to use renewable energies are aiming the same goal, which is the generation of the electrical energy in clean way. However, those can only work with some limited conditions, for instance of the specified weather, location and etc. Especially for the efficient smart–grid networks based on these resources, it is highly important for the large–scale energy storage devices such as the energy storage systems (ESS) to properly store the over–generated electricity in appropriate conditions for the energy deficient state.

In addition for the case of petroleum oil, it is reported that the considerable amounts of oil is being consumed by the vehicles based on the internal combustion engine.[3] To replace the conventional vehicles which is evolved for about a century, a number of efforts is conducted to develop the electric vehicles (EV).[5] For the popularization of EV to public, it is required for many key technologies to be researched, but the main hurdle for commercialization is the batteries to store the electrical energy which is related to the EV's mileage.

The conventional vehicles have maximum coverage of about over 500 km, and it is also quite convenient to refuel within a few minutes. However, now for EVs, they have only about 100~200 km of mileage per single full charge of batteries, and it takes longer time to recharge.[6] These problems compared to the conventional vehicles is necessary to be solved, so it is obvious that the batteries with large energy densities should be developed to enhance the practical usability of EV.

These alternatives can also reduce the cost of maintenance for such heavy applications. Although the initial expenses to introduce the applications are not low–priced, the total cost including the price of products and maintaining expense for long–term period is cheaper if we count the longer life cycles of those applications.

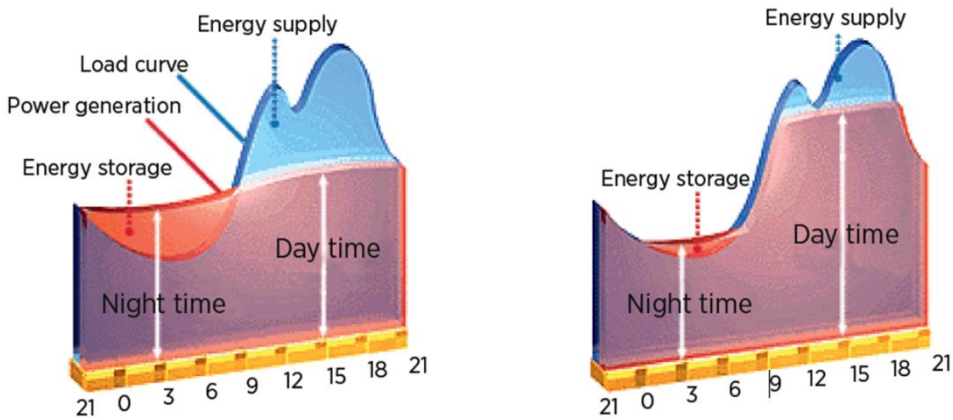

Figure 1–4. Illustration of energy supply shift based on ESS which is connected to the smart–grid networks. Copyright © IRENA 2015.[4]

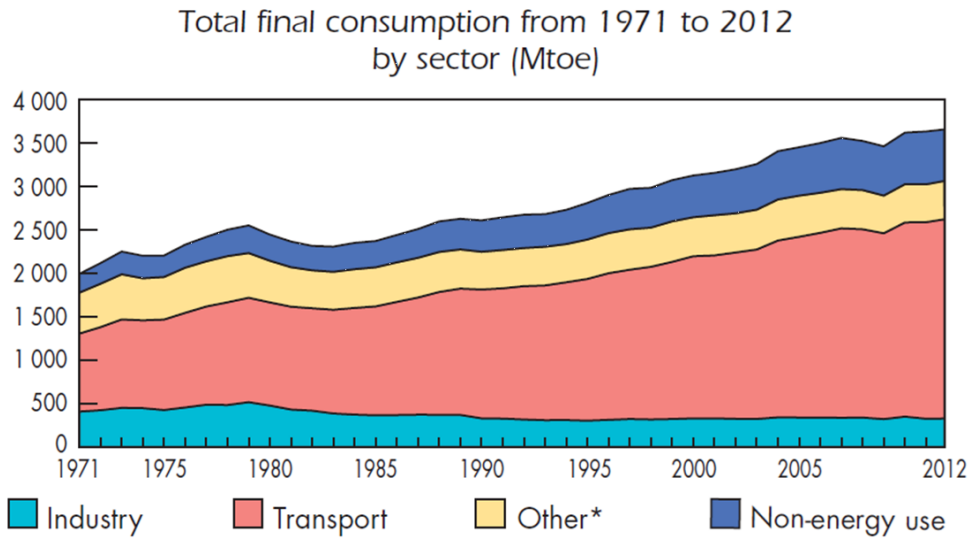

Figure 1–5. Total final consumption of petroleum oil by sectors. Based on IEA data from *Key World Energy Statistics 2014* © OECD/IEA 2014, IEA Publishing. License: *https://www.iea.org/t&c/termsandconditions/#d.en.261 26.*[3]

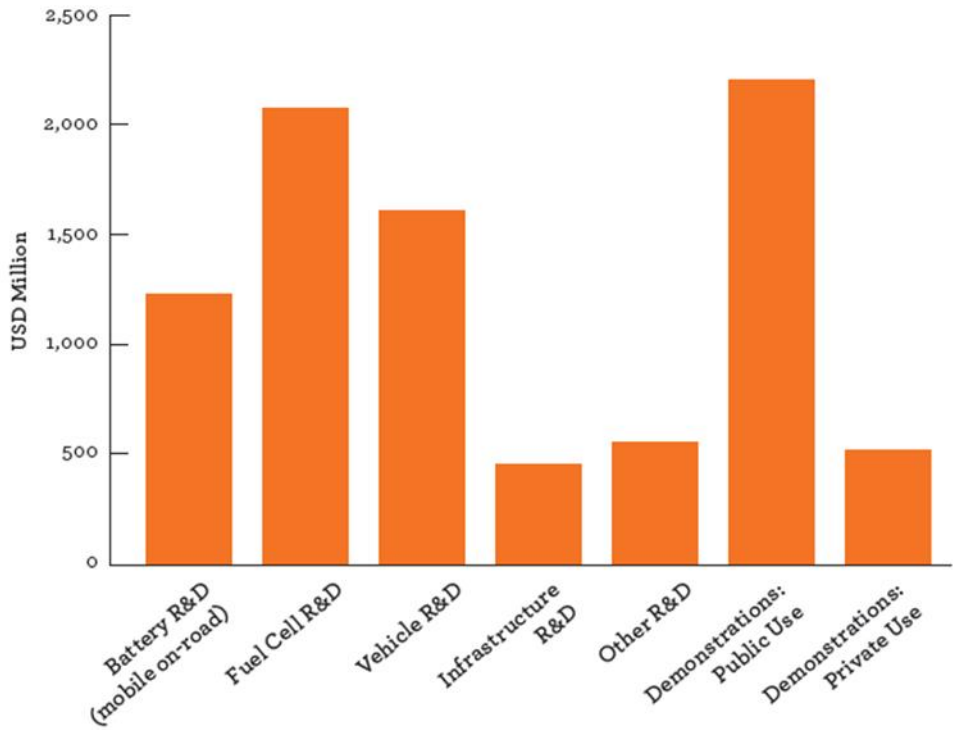

Figure 1–6. Breakdown of R&D spending for EV by countries. Based on IEA data from *Global EV Outlook: Understanding the Electric Vehicle Landscape to 2020* © OECD/IEA 2013, IEA Publishing. License: https://www.iea.org/t&c/termsandconditions/#d.en.26126.[5]

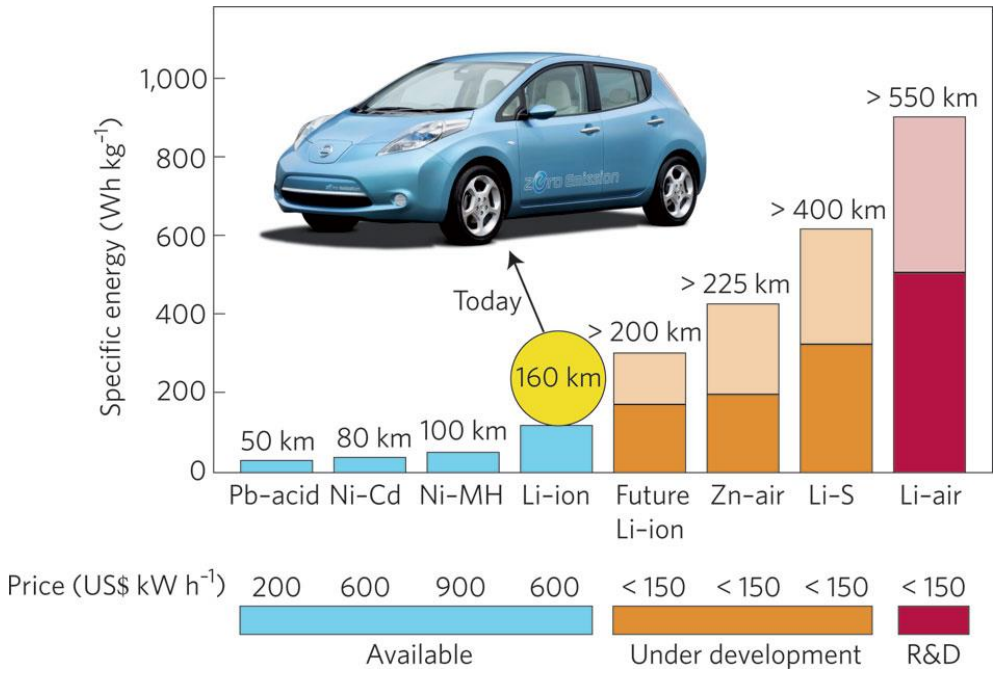

Figure 1–7. Practical specific energies for some rechargeable batteries, along with estimated driving distances and pack prices. Adapted by permission from Macmillan Publishers Ltd: Bruce, P.G., *et al.*, *Li–O_2 and Li–S batteries with high energy storage.* Nature Materials, 2012. **11**(1): p. 19–29. [6], copyright 2012

1.1.3 Technological / Engineering Background

Recently, the rechargeable lithium–ion batteries (LIB) is replacing the conventional energy storage devices such as batteries for lead–acid and metal–hydride. LIB has shown better properties compared to the former batteries in terms of the energy density, power density, cycleability and etc. However as the reasons stated above, the energy densities of current LIB are still insufficient to support the large EV and ESS, so the capacities of batteries should be further enhanced to satisfy the demands.

1.2 Metal–air batteries

1.2.1 Background

The energy storage devices have gotten huge attentions to properly use the renewable energy resources. However, the impediment for paradigm–shift to the utilizations of sustainable energy is the low energy densities of the conventional rechargeable battery systems. For this concern, the metal–air batteries with the large theoretical capacities, which exclude of the transition metal components from its charge reservoirs, were suggested and researched for about a couple of decades.

1.2.2 Working Principle

Metal–air batteries are commonly consisted with layers of alkali metal anode (Li, Na, K, Zn, Al, Si and etc) / electrolyte (nonaqueous, aqueous) / porous air cathode (carbon, metallic transition metal oxide), which is quite similar with that of LIB. The cathode side is opened to intake the supplied gas (O_2, CO_2, SO_2 and etc). However, the main difference of the metal–air cells with LIB is the charge storing reactions. Normally, the electrochemistry of LIB is the intercalation or conversion based redox reactions, but the fundamental reactions in metal–air batteries are the deposition / dissolution redox reactions on the active surface sites. The followed explanations will be provided based on the exclusion of various side reactions, but ideal redox electrochemical reactions, and in the oxygen atmosphere.

For the discharge reaction, firstly, the dissolved oxygen gas might be reduced on the surface of electrode. Consequently, the reduced oxygen (oxygen radical or superoxide anion: O_2^-) reacts with the alkali metal cations such as Li^+ or Na^+ to form the intermediate alkali metal superoxides. According to the alkali metal, the intermediate species can further react with

the environment (additional reduction or disproportionation). This procedure is highly correlated with the thermodynamics and kinetics of the metal–air electrochemistry. With this series of reactions, the final form of discharge products (alkali metal superoxide or peroxide) can be concluded.

For the charge reactions, the decomposition of discharge product is occurred. However, the reaction path can be differed compared to the discharge depending on the class of products. In general, the alkali metal superoxides are decomposed with the opposite reaction paths of the discharge process, but the alkali metal peroxides involve the different reaction paths with showing the huge charge overpotentials.

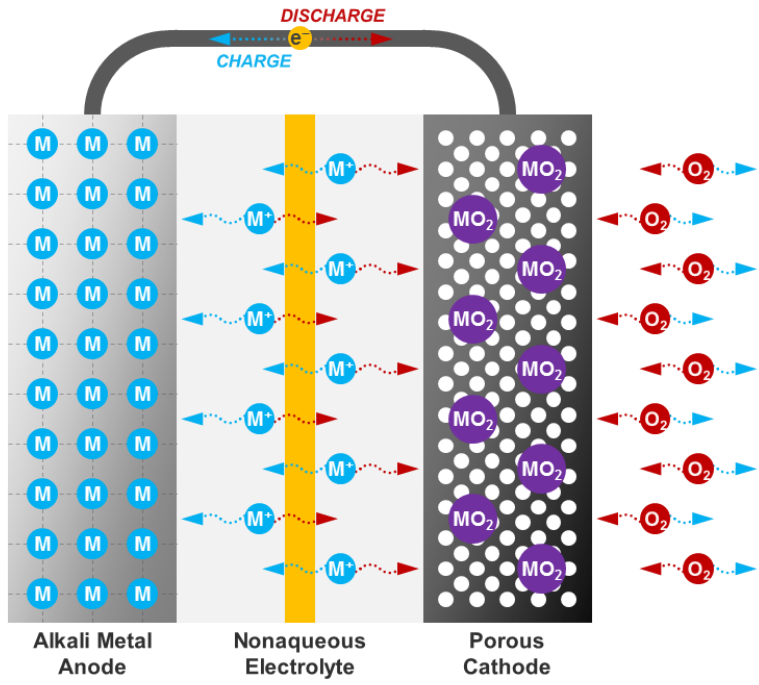

Figure 1–8. Schematics representing the working principles of metal–air batteries.

Cell reaction	V	Wh/kg	mAh/g	Wh/L	mAh/cm^3
2 Li + 1/2 O_2 ↔ Li_2O	2.91	5216	1794	10501	3606
2 Li + O_2 ↔ Li_2O_2	2.96	3456	1168	7983	2698
2 Na + 1/2 O_2 ↔ Na_2O	2.77	1687	462	3828	1968
2 Na + O_2 ↔ Na_2O_2	1.95	1602	867	4493	1936
Na + O_2 ↔ NaO_2	2.33	1105	689	2431	1074

Table 1–1. Calculated values for Li–O_2 and Na–O_2 batteries with a metal anode. Values for the gravimetric energy densities are given without and including the weight of oxygen. All other values given refer to the discharged state. Adelhelm, P., *et al., From lithium to sodium: Cell chemistry of room temperature sodium–air and sodium–sulfur batteries.* Beilstein Journal of Nanotechnology, 2015. **6**(1): p. 1016–1055. is licensed under CC BY 2.0.[1]

1.2.3 Li–O_2 Batteries: Currently Highlighted

Among some numbers of metals to construct the system, the most of researches were focused on the lithium–oxygen (Li–O_2) electrochemistry with the basis of common LIB. The Li–O_2 cell utilizes the formation / decomposition reactions of insulating lithium peroxide (Li_2O_2) at 2.96 V vs. Li/Li^+. It shows the superior theoretical capacity of 3,458 Wh kg^{-1}, which is several folds compared to that of Li–ion batteries. In spite of this virtue of capacities, the low cycle efficiency of Li–O_2 cells were the drawback for the feasibility of the electrochemical system.[6–8] The main reasons for the poor cycle life of Li–O_2 cells were identified that due to the large charge overpotential, which is over 1 V accompanying the various side reactions. Those undesired reactions involves the electrolyte decomposition or the reactions on the interfaces of the product/carbon or the product/electrolyte.[9–11] Thus, it is regarded that the electrolyte degradations and the passivation of the active reaction sites with the accumulated byproducts after several cycles hindered the reversibility of Li–O_2 electrochemical reactions. To overcome these obstacles of Li–O_2 cells, a number of studies were carried out including about the development of catalysts or redox–mediators for

OER,[12–14] and the introductions of the non–carbon based gas–cathodes such as a metallic transition metal oxides or carbides.[15–17] However, it seems that the stability of the Li–O_2 system still stuck in the hurdle, so it was necessary to propose another breakthrough for the remarkable enhancement of the reversibility for the metal–air battery systems.

Recently, it was reported that the solvating environment could altering the reaction paths and the stability of the intermediate species such as a lithium superoxide (LiO_2).[18, 19] It was believed that LiO_2 is a precedent phase with the direct reaction of Li and superoxide anion (reduced oxygen: O_2^-), which might be transformed to Li_2O_2 with the additional reduction of Li ion (electrochemical reaction: surface mechanism) or the disproportionation of O_2 molecule (chemical reaction: solution mechanism). Although there were some papers which instantly identified LiO_2, it has been known as an extremely unstable phase so that hard to characterize in detail. However, in the rich conditions of solvate, such as a high donor number of electrolyte solvent or a high concentration of solvating agent, it was observed that LiO_2 might be dissolved into the electrolyte and promote the solution reaction for the product transition to Li_2O_2. Otherwise, it was shown that LiO_2 was

relatively stable with the low solubility, and followed the surface reaction to form Li_2O_2 in the conditions of desolvate. Those natures affected to the capacities and the morphology of reaction products. With the embrace of the other literatures including calculations for the conductivity of Li_2O_2, it is obvious that the dominant reaction in the normal experimental conditions might be the solution reactions.

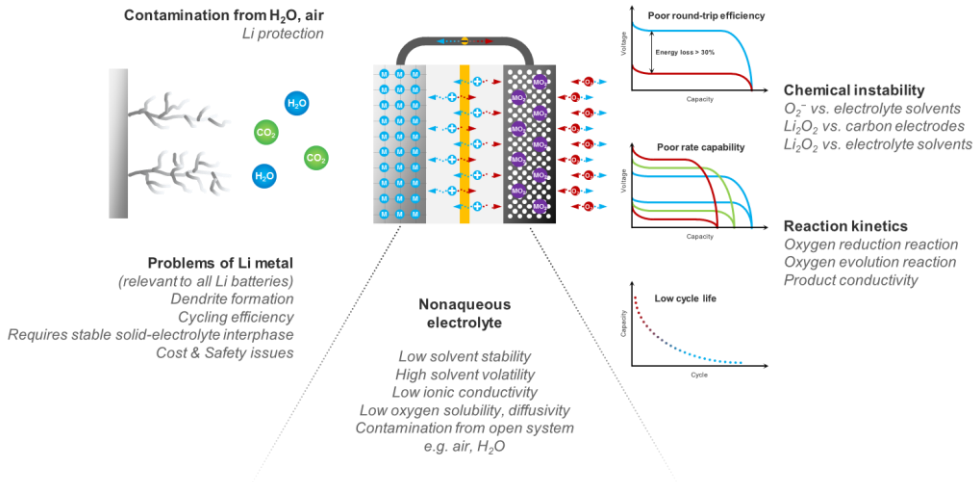

Figure 1–9. Challenges facing the non–aqueous Li–O_2 battery. Reprinted by permission from Macmillan Publishers Ltd: Bruce, P.G., *et al.*, *Li–O_2 and Li–S batteries with high energy storage.* Nature Materials, 2012. **11**(1): p. 19–29. [6], copyright 2012

1.2.4 $Na–O_2$ Batteries: Potentials to be Further Advanced

Meanwhile, as an alternatives, the sodium (Na) has been introduced to replace Li electrochemistry with a few perspectives. Commonly until now, Na–ion batteries were highlighted with the lower cost compared to that of Li in the economic point of view. It is also facile to substitute Li to Na in the intercalation–based cells, because of the similar atomic properties triggered from their vertically neighboring places in the periodic table. However, the relatively bigger ionic size of Na inhibited the performances (energy density, power capability) for the rechargeable battery systems.

As in the Na–ion batteries, analogous efforts were tried for the $Na–O_2$ electrochemistry.[20–22] Considering the large capacities which need more charge carriers in the metal–air batteries, the idea for switching from Li to Na was reasonable. Moreover, it seems that the $Na–O_2$ cells involves more diversities of reactions compared to the $Li–O_2$ cells.[1] In the early stages of research for the $Na–O_2$ cells, it was reported that sodium peroxide (Na_2O_2) was formed as similar to the $Li–O_2$ cells.[23] However, the electrochemical properties (charge overpotential, cycle life) of those cells were not differed

with that of Li system. Besides unlike with the former literatures, Hartmann *et al.* reported the formation/decomposition of sodium superoxide (NaO_2) in Na–O_2 batteries, which showed the extremely low charge overpotential (~ 0.2 V).[21, 24] The discharge products were well–defined cubic crystals with a micrometer size. This unique phenomena represented that the reaction mechanisms might be fairly different with the Li–O_2 cells. The followed papers confirmed that this reactions were much cleaner than the common Li–O_2 reactions. Thus, it was regarded that the redox reaction of NaO_2 is a promising alternative reaction with the perspective of not only the cost of materials, but also the ideality of fundamental electrochemistry. Furthermore, some groups including us reported the discharge product as sodium peroxide dihydrate ($Na_2O_2 \cdot 2H_2O$) for Na–O_2 batteries.[22, 25, 26] It was understand that those product might be formed from Na_2O_2 and unauthentic trace of water, which implies the chemical side reactions were dominantly occurred. The characteristics of the systems were alike to the literatures for Na_2O_2, except for the charge profile with the definite 3–step regions.

Lately, it was reported that the protons (H^+) could contribute as a phase–transfer catalysis for O_2^- in Na–O_2 batteries.[27] With the H^+–rich conditions,

the capacities of cells were enhanced according to the growth of NaO_2 crystallites. This reaction could be indexed as a solution reaction according to the classifications in Li–O_2 electrochemistry. Also, very recent paper found that the current rate might influence to the nucleation and growth of NaO_2, which implied the kinetics of solution reactions might be important in Na–O_2 reactions.[28] In terms of the stoichiometry, LiO_2 and NaO_2 is in the same group of alkali metal superoxides, so that is reasonable to share the chemical characteristics. Thus, it is possible for the redox reactions of NaO_2 to be identical to that of Li–O_2 cells.

3 **Li** Lithium 6.94	vs.	11 **Na** Sodium 22.99	**Cons**: Even Na batteries have lower gravimetric energy densities than Li batteries *Li_2O_2 (1168mAh/g) vs. Na_2O_2 (689 mAh/g)*
6,600	**Price of carbonate salt in 2014 (USD/ton)**	138 (natural) 290 (synthetic)	
16	**Crustal abundance (ppm)**	23,600	
58	**Reserve distribution (%)**	Unknown	**Pros**: Na is sufficiently cheaper than Li due to its abundance, so it is appropriate for the large scale energy storage devices such as metal–air batteries
Chile China Australia	**Top 3 reserve holders**	Unknown	
67.5	**Political stability of top reserve holder**	Unknown	
<10	**Recycling rate (%)**	Unknown	
High	**Substitutability**	Unknown	**Pros**: Na also has similar chemistry with Li triggered from neighboring in periodic table
−570.954 (Li_2O_2)	**Theoretical Gibbs formation energy of oxides (kJ/mol)**	−449.627 (Na_2O_2)	**Pros**: Na–O_2 batteries have potentials to be charged with lower voltage compared to Li–O_2 batteries

Table 1–2. Comparison of Li vs. Na in the view points of sustainability and feasibility for the metal–air batteries.[29–32]

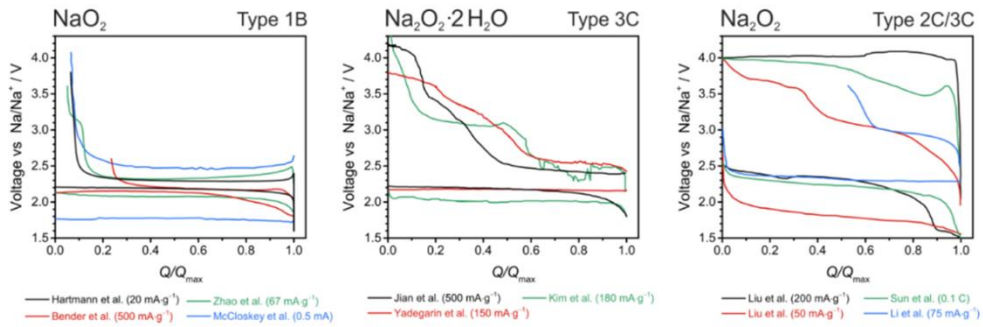

Figure 1–10. Literature overview on different studies of Na–O_2 cells. The comparison shows the voltage profile of the first cycle. Adelhelm, P., *et al.*, *From lithium to sodium: Cell chemistry of room temperature sodium–air and sodium–sulfur batteries.* Beilstein Journal of Nanotechnology, 2015. **6**(1): p. 1016–1055. is licensed under CC BY 2.0.[1]

1.3 Purpose of this research

Even there are a number of benefits for Na–O_2 batteries in fundamental and practical perspectives, it is still obvious that a few remained problems should be solved. As already reported, Li–O_2 and Na–O_2 reactions are dissimilar despite of their simple difference of alkali metal compounds. It has been reported for the conflict observations for the discharge products of Na–O_2 cells, so the fundamental behaviors are under debate as ever. Thus to achieve the further advancement of Na–O_2 batteries, the basics of electrochemical and chemical reactions should be fully understand to improve the electrochemical properties of Na–O_2 reactions. Then, to the metal–air battery society, these consequences might offer the insight and guidance for the managing kinetics of the intertwined reactions.

1.4 References

1. Adelhelm, P., *et al.*, *From lithium to sodium: Cell chemistry of room temperature sodium–air and sodium–sulfur batteries.* Beilstein Journal of Nanotechnology, 2015. **6**(1): p. 1016–1055.

2. Pachauri, R.K., *et al.*, *Climate Change 2014: Synthesis Report. Contribution of Working Groups I, II and III to the Fifth Assessment Report of the Intergovernmental Panel on Climate Change*, R.K. Pachauri and M.R. Allen, Editors. 2014, IPCC: Geneva, Switzerland.

3. Birol, F., *Key World Energy Statistics 2014*, F. Birol, Editor 2014, IEA: Paris, France.

4. Kempener, R. and E. Borden, *BATTERY STORAGE FOR RENEWABLES: MARKET STATUS AND TECHNOLOGY OUTLOOK*, R. Kempener and E. Borden, Editors. 2015: Abu Dhabi, United Arab Emirates.

5. Trigg, T. and P. Telleen, *Global EV Outlook*, in *Understanding the Electric Vehicle Landscape to 2020*, T. Trigg and P. Telleen, Editors. 2013, EVI, IEA: Paris, France.

6. Bruce, P.G., *et al.*, *Li–O_2 and Li–S batteries with high energy storage.* Nature Materials, 2012. **11**(1): p. 19–29.

7. Débart, A., *et al.*, *α–MnO_2 Nanowires: A Catalyst for the O_2 Electrode in Rechargeable Lithium Batteries.* Angewandte Chemie–International Edition, 2008. **47**(24): p. 4521–4524.

8. Freunberger, S.A., *et al.*, *The lithium–oxygen battery with ether–based electrolytes.* Angewandte Chemie – International Edition, 2011. **50**(37): p. 8609–8613.

9. Ottakam Thotiyl, M.M., *et al.*, *The Carbon Electrode in Nonaqueous Li–O_2 Cells.* Journal of the American Chemical Society, 2013. **135**(1): p. 494–500.

10. McCloskey, B.D., *et al.*, *Solvents critical role in nonaqueous Lithium–Oxygen battery electrochemistry.* Journal of Physical Chemistry Letters, 2011. **2**(10): p. 1161–1166.

11. McCloskey, B.D., *et al.*, *Twin problems of interfacial carbonate formation in nonaqueous Li–O_2 batteries.* Journal of Physical Chemistry Letters, 2012. **3**(8): p. 997–1001.

12. Chen, Y., *et al.*, *Charging a Li–O_2 battery using a redox mediator.* Nature Chemistry, 2013. **5**(6): p. 489–494.

13. Lim, H.–D., *et al.*, *Superior Rechargeability and Efficiency of Lithium–Oxygen Batteries: Hierarchical Air Electrode Architecture Combined with a Soluble Catalyst.* Angewandte Chemie–International Edition, 2014. **126**(15): p. 4007–4012.

14. Bergner, B.J., *et al.*, *TEMPO: A Mobile Catalyst for Rechargeable Li–O_2 Batteries.* Journal of the American Chemical Society, 2014. **136**(42): p. 15054–15064.

15. Ottakam Thotiyl, M.M., *et al., A stable cathode for the aprotic Li–O_2 battery.* Nature Materials, 2013. **12**(11): p. 1050–1056.

16. Kundu, D., *et al., Nanostructured metal carbides for aprotic Li–O_2 batteries: New insights into interfacial reactions and cathode stability.* Journal of Physical Chemistry Letters, 2015. **6**(12): p. 2252–2258.

17. Riaz, A., *et al., Carbon–free cobalt oxide cathodes with tunable nanoarchitectures for rechargeable lithium–oxygen batteries.* Chemical Communications, 2013. **49**(53): p. 5984–5986.

18. Johnson, L., *et al., The role of LiO_2 solubility in O_2 reduction in aprotic solvents and its consequences for Li–O_2 batteries.* Nature Chemistry, 2014. **6**(12): p. 1091–1099.

19. Aetukuri, N.B., *et al., Solvating additives drive solution–mediated electrochemistry and enhance toroid growth in non–aqueous Li–O_2 batteries.* Nature Chemistry, 2015. **7**(1): p. 50–56.

20. Li, Y., *et al.*, *Superior catalytic activity of nitrogen–doped graphene cathodes for high energy capacity sodium–air batteries.* Chemical Communications, 2013. **49**(100): p. 11731–11733.

21. Hartmann, P., *et al.*, *A rechargeable room–temperature sodium superoxide (NaO_2) battery.* Nature Materials, 2012. **12**(3): p. 228–232.

22. Kim, J., *et al.*, *Sodium–oxygen batteries with alkyl–carbonate and ether based electrolytes.* Physical Chemistry Chemical Physics, 2013. **15**(10): p. 3623–3629.

23. Sun, Q., Y. Yang, and Z.W. Fu, *Electrochemical properties of room temperature sodium–air batteries with non–aqueous electrolyte.* Electrochemistry Communications, 2012. **16**(1): p. 22–25.

24. Hartmann, P., *et al.*, *A comprehensive study on the cell chemistry of the sodium superoxide (NaO_2) battery.* Physical Chemistry Chemical Physics, 2013. **15**(28): p. 11661–11672.

25. Yadegari, H., *et al.*, *On rechargeability and reaction kinetics of sodium–air batteries.* Energy & Environmental Science, 2014. **7**(11): p. 3747–3757.

26. Zhao, N., C. Li, and X. Guo, *Long–life Na–O_2 batteries with high energy efficiency enabled by electrochemically splitting NaO_2 at a low overpotential.* Physical Chemistry Chemical Physics, 2014. **16**(29): p. 15646–15652.

27. Xia, C., *et al.*, *The critical role of phase–transfer catalysis in aprotic sodium–oxygen batteries.* Nature Chemistry, 2015. **7**(6): p. 496–501.

28. Ortiz–Vitoriano, N., *et al.*, *Rate–Dependent Nucleation and Growth of NaO_2 in Na–O_2 Batteries.* The Journal of Physical Chemistry Letters, 2015. **6**(13): p. 2636–2643.

29. Website. *http://www.rsc.org/periodic–table*. 2015.

30. Jaskula, B.W., *Lithium*, in *Mineral Commodity Summaries*, B.W. Jaskula, Editor 2015, U.S. Geological Survey: Reston, Virginia, USA.

31. Bolen, W.P., *Soda Ash*, in *Mineral Commodity Summaries*, W.P. Bolen, Editor 2015, U.S. Geological Survey: Reston, Virginia, USA.

32. Baysinger, G., *CRC Handbook of Chemistry and Physics*2012: Rensselaer Polytechnic Institute.

Chapter 2. Sodium–Oxygen Batteries with Alkyl–carbonate and Ether based Electrolytes

(The content of this chapter has been published in *Physical Chemistry Chemical Physics*. Reprinted with permission from [J. Kim *et al.*, *Phys. Chem. Chem. Phys.*, **15**, 3623–3629 (2013); DOI: 10.1039/C3CP43225D].

2.1 Introduction

Environmental and sustainable energy concerns have led to intensive efforts to find ways to minimize the use of fossil fuels. In the paradigm shift from fossil fuels to renewable energy resources such as solar, wind, and geothermal power generation, the key to success lies in the development of reliable large–scale energy storage devices. The lithium–oxygen battery has been suggested as one solution to the energy storage issue because of its exceptionally high energy storage capacity. Since lithium ions can react directly with oxygen in ambient air without heavy transition metal component, the theoretical energy density of the lithium–oxygen battery can be several times higher than that of

conventional lithium–ion batteries.[1–8] However, there is concern that the amount of available lithium resources would be insufficient to satisfy the increased demand due to batteries based on lithium chemistry.[9, 10] Although this prediction involves significant assumptions, and there is ample evidence that this is not a cause for immediate concern, it indicates that the cost of lithium may increase as demand increases.[9, 11]

On the other hand, sodium is abundant and inexpensive because it can be readily extracted from seawater. Furthermore, sodium is placed right below lithium in the periodic table; they share many similar chemical properties. In this respect, sodium–ion batteries, whose fundamental principle is identical to that of lithium–ion batteries, are already regarded as one of the more promising alternative battery systems.[9, 12, 13] Analogous to this trend, a few attempts have been made to fabricate sodium–oxygen batteries.[14–16] Peled *et al.* reported high–temperature (above 100 ℃) sodium–oxygen batteries using molten sodium.[14] Sun *et al.* also reported sodium–air batteries with a carbonate electrolyte that operated at room temperature.[15] Also, Hartmann *et al.* very recently have demonstrated sodium–air batteries using a non–carbonated electrolyte with the main discharge product as

sodium superoxide (NaO_2).[16] Although these reports proved the feasibility of sodium–oxygen batteries, the detailed electrochemical reaction mechanism is not well understood. Moreover, recent studies of lithium–oxygen batteries have revealed that using a carbonate based electrolyte leads to irreversible formation of lithium carbonate as a main discharge product, whereas lithium oxides are produced when a non–carbonate based electrolyte is used.[3, 4, 17–20] In this respect, the reaction mechanism of the sodium–oxygen cell needs to be investigated with a clear distinction between types of electrolytes.

Here, we fabricated sodium–oxygen batteries based on two types of electrolytes to investigate the electrochemical reactions that occur during cycling. It was found that the formation and decomposition of sodium carbonate is responsible for the cyclic process in the carbonate based cell. On the contrary, hydrated sodium oxides and sodium hydroxide were the main reaction products in the non–carbonate electrolyte system. This behavior is similar to the reaction mechanism that reported for the lithium–oxygen battery, except that for the sodium–oxygen battery, the hydrated phases are preferred because of the strongly hygroscopic nature of sodium oxides when exposed to water which is also produced during decomposition of the electrolyte.

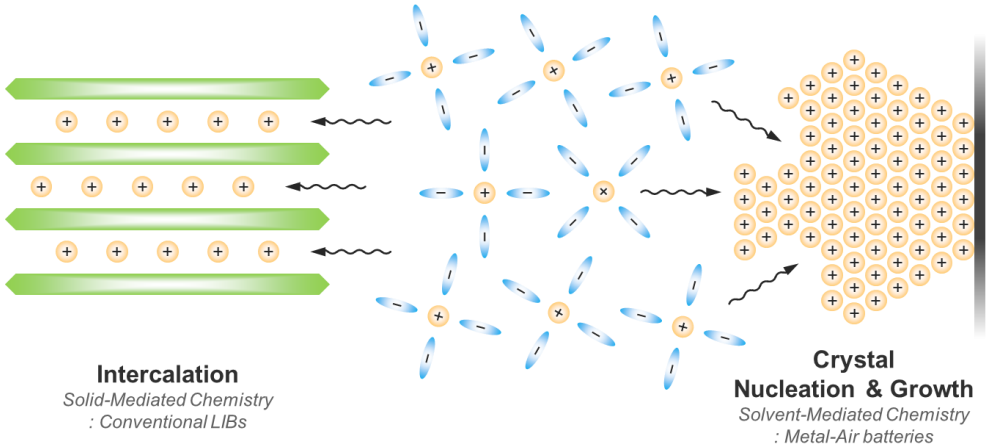

Figure 2–1. Importance of the electrolyte solvent in metal–air batteries, because the discharge products can be affected by the solvent in terms of size, morphology, composition, distribution, crystallinity and etc.

	EC Ethylene Carbonate	**PC** Propylene Carbonate	**DMC** Dimethyl Carbonate	**DME** Dimethoxy Ethane	**DEGDME** Diethylene Glycol Dimethyl Ether	**TEGDME** Tetraethylene Glycol Dimethyl Ether
Molecular Weight (g/mol)	88.06	102.09	90.08	90.12	134.18	222.28
Melting Point (˚C)	36.4	−48.8	4.6	−58	−64	−46
Boiling Point (˚C)	248	242	91	84	162	216
Flash Point (˚C)	160	132	18	0	57	111
Viscosity (cP, 25˚C)	1.9	2.53	0.59	0.46	1.06	3.39
Dielectric Constant (25˚C)	89.78	64.92	3.107	7.18	7.4	7.53
Diffusion Cofficient (10^{-10} m^2/s)	8.0	5.8	26	31	13	6.1
Ionic Conductivity (mS/cm)	8.3	5.2	2.7	8.9	4.5	2.0
Dipole Moment (D)	4.61	4.81	0.76	1.15	1.91	2.45
Acceptor Number (Donor Number)	(16.4)	18.3 (15.1)		10.9 (18.6)	9.9 (19.2)	10.5 (14)

Table 2–1. Comparison of the organic solvent for conventional LIBs in terms of the physicochemical characteristics.[21–26]

2.2 Experimental

The sodium metal (Sigma–Aldrich) anode was prepared by milling a chunk of sodium after removing the residual surface oxides. All of the sample preparation was carried out in an argon–filled glove box. The porous oxygen cathode was fabricated by coating carbon paste (Ketjen Black and Kynar 2801) as a carbon support with binder at a 9:1 ratio in N–methy–2–pyrrolidone (NMP, Sigma–Aldrich, 99.5%) on a nickel–mesh current collector (0.5 inch diameter). The cathode was dried at 120 ℃ for 1 h in vacuum. Two types of electrolytes were used: propylene carbonate (PC, Sigma–Aldrich, 99.7%) as the carbonate electrolyte and tetraethylene glycol dimethyl ether (TEGDME, Sigma–Aldrich, 99%) as the non–carbonate electrolyte. The amounts of carbon loading were 0.779 mg (0.615 mg/cm^2) for PC electrolyte and 0.698 mg (0.551 mg/cm^2) for TEGDME electrolyte. 1 M of sodium perchlorate ($NaClO_4$, Sigma–Aldrich) was dissolved in both electrolytes. The cells were fabricated in Swagelok® –type air battery system using a glass–fiber separator (Whatman® GF/D microfiber filter paper, 2.7 μm pore size) as reported in our previous work.6 Electrochemical testing (WBCS 3000, WonA Tech, Korea) was performed within 1.8 ~ 4.5 V range

at a current density of 0.1 mA/cm^2 in oxygen flowing at 1 atm. Capacities were calculated based on the carbon weight. The galvanostatic intermittent titration technique (GITT) was carried out by applying 20 minutes of constant current followed by 3 hours of resting.

The electrodes were collected after charge or discharge, washed with the corresponding solvents (PC or TEGDME) and wiped out for further characterizations. The X–ray diffraction (XRD, D8–Advance, Bruker, Germany) spectra of electrodes were measured within 2θ of 25 to 42.5 ° at a scan rate of 0.5 °/min in an air–tight holder to prevent any side reactions caused by the ambient atmosphere. The Fourier transform infrared (FTIR, FT–IR–4200, JASCO, Japan) spectra of samples pelletized with KBr powder were measured in an argon atmosphere from 400 to 4000 cm^{-1}. Raman spectroscopy (LabRam Aramis, Horiba Jobin Yvon, France) of electrodes were measured within 600 to 1750 cm^{-1} at 600 grating/mm for 300 seconds. X–ray photoelectron spectroscopies (XPS, PHI 5000 VersaProbe II, Ulvac–PHI, Inc., Japan) of samples were obtained with pass energy of 23.5 eV, step of 0.05 eV, and 50 ms/step of scanning time.

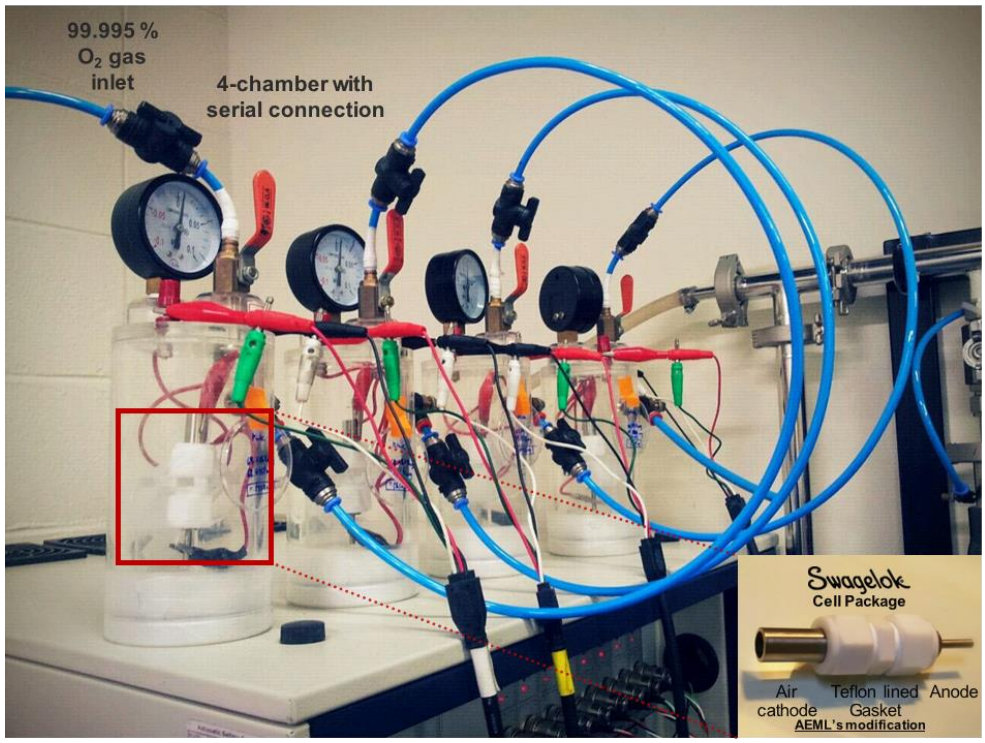

Figure 2–2. Experimental setup for galvanostatic cycling of Na–O_2 batteries. Serial connection of O_2 flowing for the individual gas–tight chambers.

2.3 Results and Discussion

2.3.1 Reactions in the carbonate based electrolyte

The galvanostatic discharge/charge profile and its cycleability of the sodium–oxygen cell having the PC electrolyte is shown in Figure 2–3. The sodium–oxygen cell could deliver a first discharge capacity of about 2800 mAh/g at ca. 2.3 V. The discharge characteristic is comparable, but slightly lower, than that of the lithium–oxygen cell (2.7 V).[3] The voltage difference corresponds well to the difference in the standard electrode potentials between lithium and sodium.[27] During the subsequent charge process, it was possible to recharge almost all of the discharged capacity. However, the polarization between charge and discharge was quite high, which could indicate either an exceptionally sluggish electrochemical reaction or the possibility of different charge and discharge reaction mechanisms.[2, 28]

The electrodes were studied by XRD following discharge or charge events to identify the electrochemical reactions that occurred during the cycle. Figure 2–4 shows that sodium carbonate (Na_2CO_3) was the main discharge product after the initial discharge until 1.8 V. This contrasts with the expected

discharge reaction in the sodium–oxygen cell, i.e., formation of Na_2O_2, but it agrees with previous reports concerning lithium–oxygen batteries with carbonate electrolytes.[3, 15] The formation of lithium carbonate (instead of Li_2O_2) in lithium–oxygen batteries is attributed primarily to degradation of the carbonate electrolyte after the first discharge.[3] We believe that a similar reaction occurred in the sodium–oxygen batteries with carbonate electrolytes, as will be discussed in detail below. The XRD peaks of the discharge products completely disappeared after the subsequent charging process. This indicated that the charge reaction involves the decomposition of sodium carbonate. Same behaviors were observed with the FTIR spectroscopies in Figure 2–5 indicating the formation and decomposition of sodium carbonate rather than sodium peroxide occurred during the initial cycling. In Figure 2–6, Raman spectra of the electrode with PC electrolyte after discharge/charge are also shown. The revealed peak along with the broad carbon background which is D and G band indicated the discharge product was mainly Na_2CO_3.[29] XPS in Figure 2–7 further exhibit the peak for binding energy of Na 1s in Na_2CO_3 environment, while both assigned spectra vanished after the charging process.[30]

The proposed reaction mechanism for sodium–oxygen batteries with PC electrolyte are illustrated in Figure 2–9. The initial degradation of PC upon the discharge is expected to be identical to the proposed mechanisms for lithium–oxygen batteries with the same electrolyte.[3] During the discharging, (1) O_2 gas reacts with the electron (e^-) supplied by the electrode to form O_2^-, which is highly reactive; (2) O_2^- attacks the ethereal C atoms of CH_2 group in PC by S_N2 substitution; and (3) the imbalance of the bonding between the two O atoms results in ring–opening of PC to form peroxo alkyl carbonate. A recent computational study revealed that these steps of degradation by the attack of O_2^- could occur.[31] (4) The unstable peroxo radical species decomposes in the presence of O_2 gas along various reaction paths,[32, 33] leading to formation of H_2O, CO_2, and some byproducts;[3] (5) the evolved CO_2 gas further reacts with the O_2^- to form an intermediate $C_2O_6^{2-}$ species[34, 35] and (6) subsequently reacts with Na^+ ions to form Na_2CO_3 with evolution of O_2 gas.

The charging process could proceed by (1) loss of Na^+ and e^- from Na_2CO_3 to form the peroxo radical species; (2) dimerization of the radical species to balance the valency and form $Na_2C_2O_6$; (3) extraction of Na^+ and e^- to (4)

decompose $Na_2C_2O_6$ to $NaCO_4^{\bullet}$ with CO_2 evolution; and finally (5) decomposition of $NaCO_4^{\bullet}$ to Na^+, O_2^-, and CO_2.[35] Additionally, (6) the evolution of highly reactive O_2^- would promote the decomposition of PC to H_2O and CO_2 again.

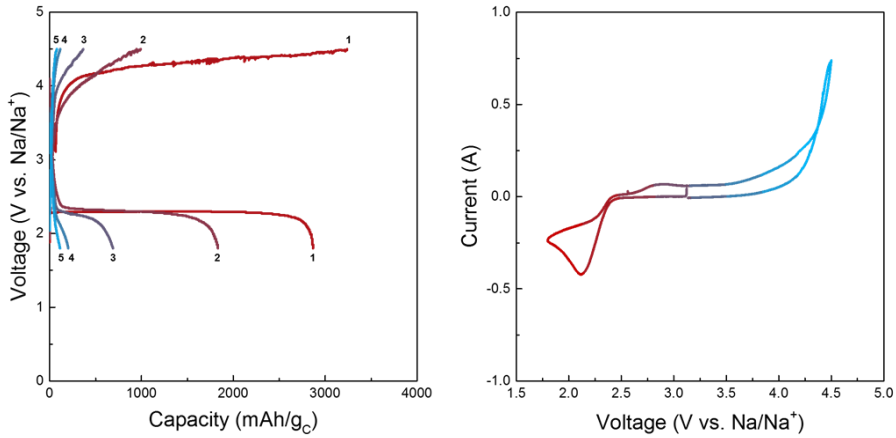

Figure 2–3. Galvanostatic discharge/charge profiles representing cycleability (left) and cyclic voltammetry with PC electrolyte (right).

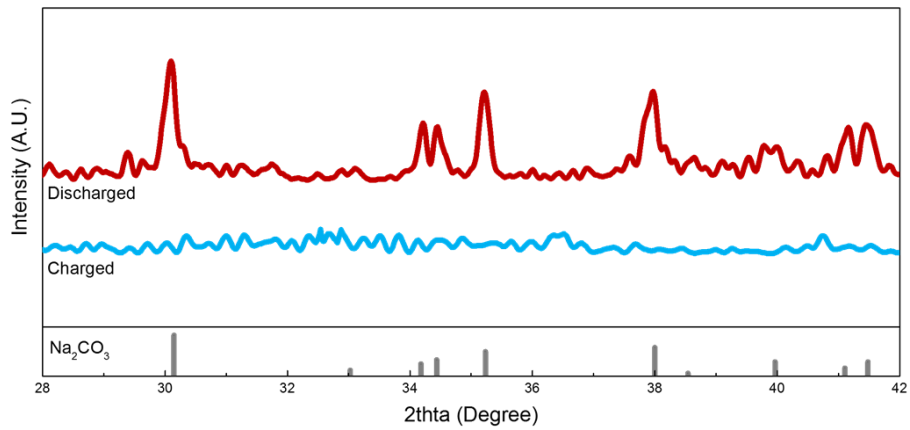

Figure 2–4. XRD measurements after the initial discharge until the 1.8 V cut–off limit and the subsequent recharging processes with PC electrolyte.

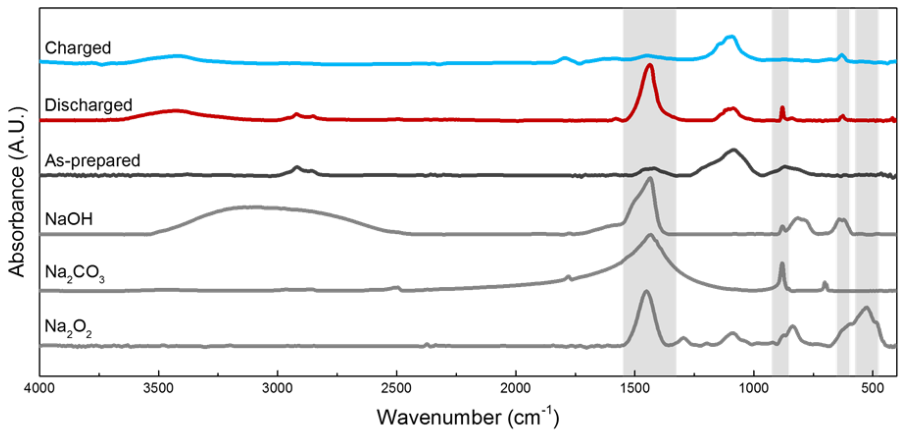

Figure 2–5. FTIR spectra after the initial discharge until the 1.8 V cut–off limit and the subsequent recharging processes with PC electrolyte.

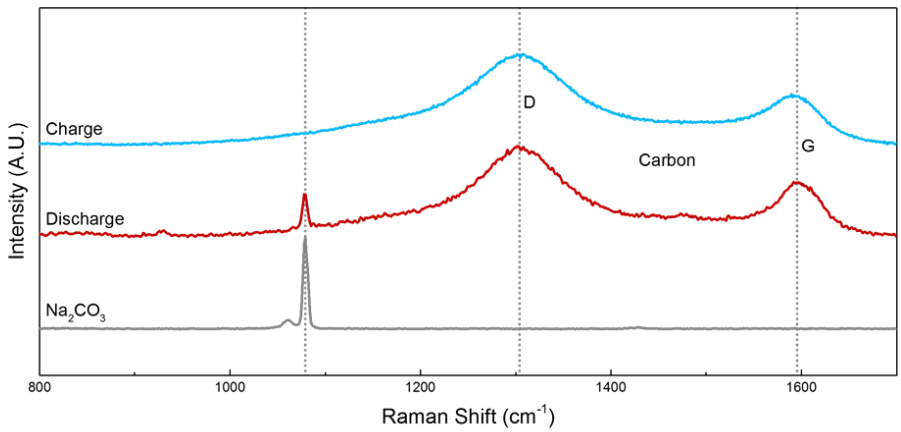

Figure 2–6. Raman spectra after the initial discharge until the 1.8 V cut–off limit and the subsequent recharging processes with PC electrolyte.

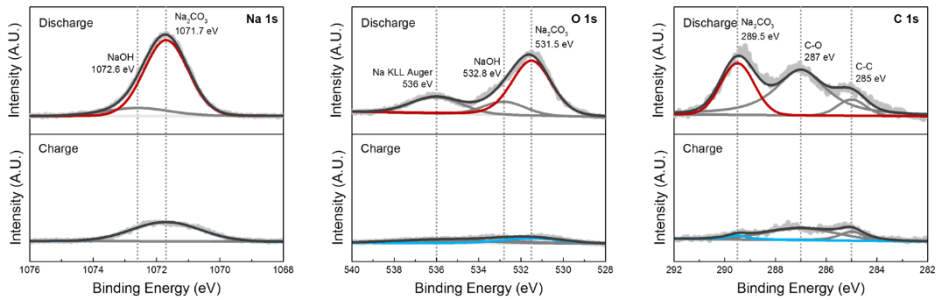

Figure 2–7. XPS measurements after the initial discharge until the 1.8 V cut–off limit and the subsequent recharging processes with PC electrolyte.

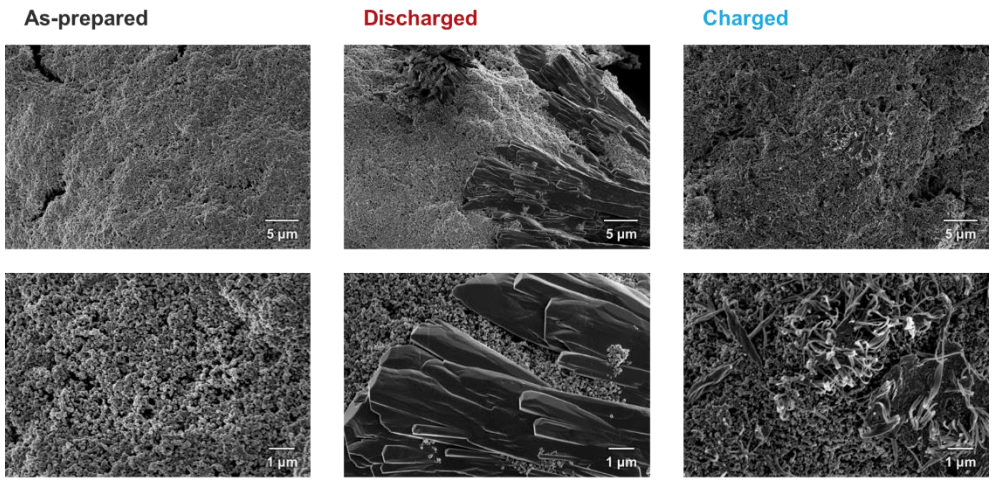

Figure 2–8. SEM images after the initial discharge until the 1.8 V cut–off limit and the subsequent recharging processes with PC electrolyte.

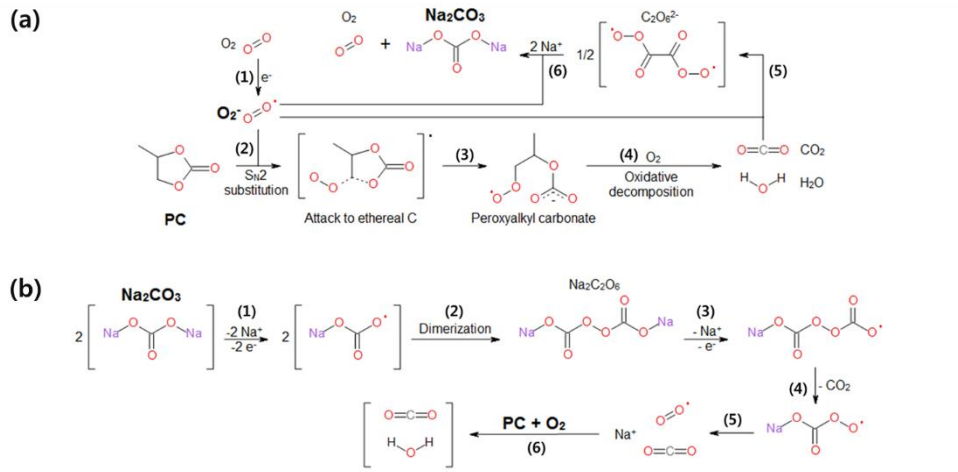

Figure 2–9. Schematic diagram of the proposed reaction mechanisms for the (a) discharging and (b) charging processes with PC electrolyte.

2.3.2 Reactions in the non–carbonate based electrolyte

The galvanostatic discharge profile and its cycleability of the sodium–oxygen cell with the TEGDME electrolyte is shown in Figure 2–10. The cell could deliver a first discharge capacity of 6000 mAh/g. This is comparable to the highest capacity reported for lithium–oxygen batteries in non–carbonate based electrolytes in the absence of catalysts.[5, 36, 37] However, the discharge potential was around 2 V, which is lower than that of the lithium–oxygen cell and even lower than that of the sodium–oxygen cell with the PC electrolyte. This implied that the electrochemical reactions occurring in the TEGDME system differed from those in the PC system. When we attempted to charge the cell galvanostatically, we observed that the voltage profile was very unstable (Figure 2–10). This undesirable behavior appeared repeatedly, even under carefully controlled test conditions. However, we could partially observe the flat voltage region of 2.5 V at the beginning of charge, which might be related to the recent report.[16] The reason for the unstable voltage profile during charge will be discussed later in relation to the reaction mechanism. Instead, we forced the cell to charge in a constant voltage (CV) mode at several voltages (2.5, 3.0, 3.5, and 4.0 V).

Figure 2–11 shows the XRD measurements of the electrodes after the first discharge and charge. The main product of the discharge event was sodium peroxide dihydrate ($Na_2O_2 \cdot 2H_2O$). A trace amount of sodium hydroxide (NaOH) was also detected. This clearly indicated that the reaction mechanism in the TEGDME system differed from that in the PC based carbonate electrolyte system, which is similar to what has been reported for lithium–oxygen batteries.[3, 4] However, the discharge product was, surprisingly, not Na_2O_2 or Na_2O, which would be analogous to Li_2O_2 or Li_2O for lithium–oxygen batteries with the same electrolyte, but the hydrated form. To exclude the possibility of any water contamination of the product from the discharge during sample handling, all the procedures were done in a dry box under high–purity argon, and the XRD measurement was repeated using a specially sealed sample holder. However, the results were the same. We note also that experiments done using an identical setup with a lithium–oxygen battery gave Li_2O_2 and not the hydrated form or LiOH. Therefore, water is assumed to have been produced by the decomposition of TEGDME electrolyte within the cell during operation and to have reacted with the sodium peroxide. The trace amount of NaOH that was detected is attributed to either the reaction between

Na_2O_2 and H_2O ($Na_2O_2 + 2\ H_2O \rightarrow 2\ NaOH + H_2O_2$) or to the decomposition of $Na_2O_2{\cdot}2H_2O$ ($Na_2O_2{\cdot}2H_2O \rightarrow 2\ NaOH + H_2O_2$).[38] In Figure 2–13 of XPS, the peak for binding energy of Na 1s in Na_2O_2 was determined after first discharge, which indicated the presence of sodium oxides.[39] FTIR spectra in Figure 2–12 also showed the characteristic peak of Na_2O_2 in the electrode after initial discharge. The peaks were eventually disappeared after the following charge.

Electrodes at different charging states were examined by XRD to investigate the reactions that occurred during the charge process as shown in Figure 2–11. The as–discharged electrode consisted of $Na_2O_2{\cdot}2H_2O$ and NaOH, but the electrode after charging at a constant 2.5 V was mainly NaOH according to the enhanced peak intensity observed for these species. Peaks for the main product from the discharge, *i.e.*, $Na_2O_2{\cdot}2H_2O$, were not observed. Charging at a higher constant voltage of 3.0 to 4.0 V completely removed all of the products from the discharging process. This is consistent with the dehydrating sequence from $Na_2O_2{\cdot}2H_2O$ to α and β phase of NaOH.[40, 41]

Based on these observations, we propose the following discharging and charging mechanisms for sodium–oxygen batteries with TEGDME electrolyte. A schematic diagram of the reaction sequence is illustrated in Figure 2–15. Upon discharging, (1) O_2 gas reacts with the e^- from the electrode to form O_2^-, which (2) attacks the electrolyte and abstracts a H atom of the CH_2 group in the TEGDME analogous to the S_N2 substitution of PC in Figure 2–15(a);[4] (3) the O_2 gas reacts further to form a highly unstable peroxo ether radical; (4) this radical decomposes in the presence of O_2 to evolve H_2O, CO_2, and some byproducts;[4] (5) meanwhile, O_2^- reacts with Na^+ ions to form NaO_2, and (6) the NaO_2 then reacts to form Na_2O_2 and O_2 gas.

Because Na_2O_2 is highly hygroscopic (in contrast to Li_2O_2),[42] it readily absorbs water molecules that were produced in the oxidative decomposition reaction (4). Thus, (7) the hydrated phase, $Na_2O_2{\cdot}2H_2O$, finally forms because the final product from the discharge is not a simple oxide but rather a hydrated phase. It is reported that Na_2O_2 have two hydrate phases which are $Na_2O_2{\cdot}2H_2O$ and $Na_2O_2{\cdot}8H_2O$.[42] If the Na_2O_2 is hygroscopic enough to react with all the H_2O from reaction 4, we can roughly estimate the relative

reaction rates for the formation of hydrate phases. Regarding the formation of $Na_2O_2 \cdot 2H_2O$ phase with 1:1 ratio of Na:H_2O, the rates of reaction (4) and (5) might be comparable, otherwise, anhydrous Na_2O_2 or $Na_2O_2 \cdot 8H_2O$ might be formed due to the corresponding range of reaction rates. It implies the severe occurrence of the reaction (4) which is the decomposition of the electrolytes. This strongly supports the poor cycleability of the ether–based sodium–oxygen system as shown in Figure 2–10(a).

The charging mechanism is substantially different than that for the lithium–oxygen cell with the same electrolyte. Upon charging, (1) $Na_2O_2 \cdot 2H_2O$ is first triggered to decompose into NaOH and H_2O_2.[42] It is not clear how the electrical charging triggers the reaction to NaOH, but the consideration of Gibbs free energy indicates that the reaction should be spontaneous.[43] The small amount of NaOH detected after the discharge may have resulted from spontaneous decomposition of $Na_2O_2 \cdot 2H_2O$. However, a substantial amount of NaOH was observed only after the charging process. Subsequently, (2) the extraction of Na from NaOH results in H_2O_2, which (3) spontaneously decomposes to H_2O and O_2.[42, 44] Multiple spontaneous decompositions occur during the charging process. We believe that these decompositions

destabilize the voltage measurement at the surface of the electrode,[5, 45] thus creating the erratic voltage profile observed during charging. Even though the discharge process of the sodium–oxygen cell with TEGDME is similar to that of the lithium–oxygen cell, the charge process is somewhat more complex because of the involvement of water in the sodium–oxygen cell. The decomposition of TEGDME has a greater influence on the reaction mechanism of the sodium–oxygen cell because of the strong hygroscopic nature of Na_2O_2.[42] This implies that identifying a stable electrolyte is very important for the further development of sodium–oxygen batteries.

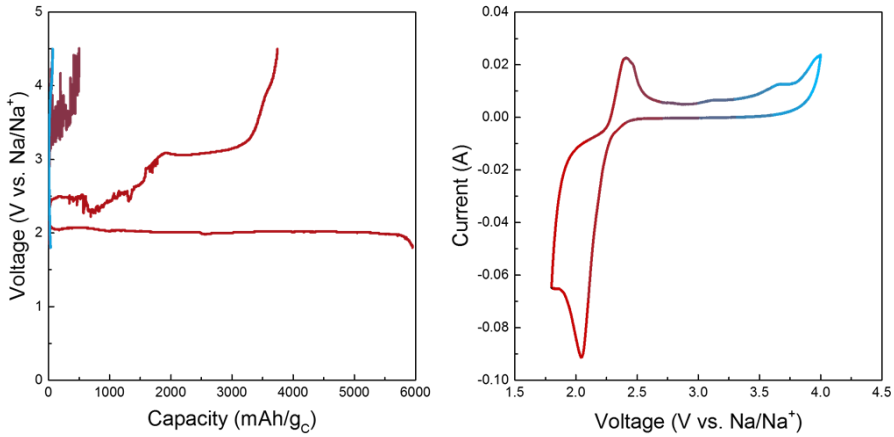

Figure 2–10. Galvanostatic discharge/charge profiles representing cycleability (left) and cyclic voltammetry for Na–O_2 battery with TEGDME electrolyte (right).

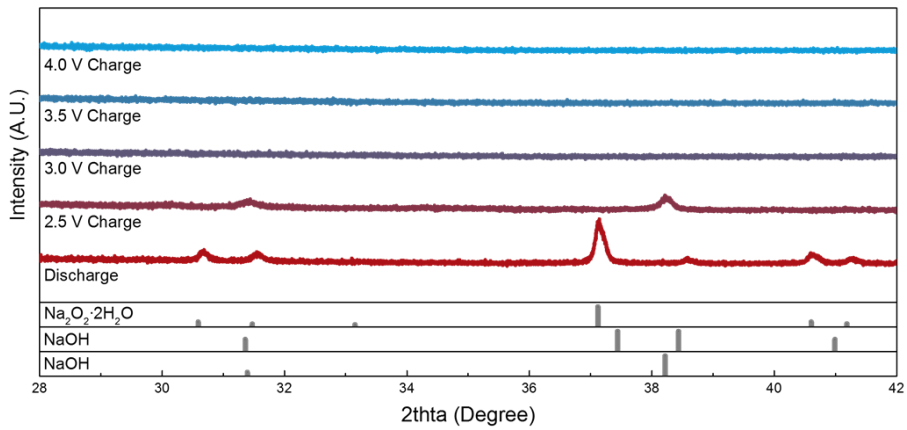

Figure 2–11. XRD measurements after the initial discharge until the 1.8 V cut–off limit and the subsequent recharging processes with TEGDME electrolyte.

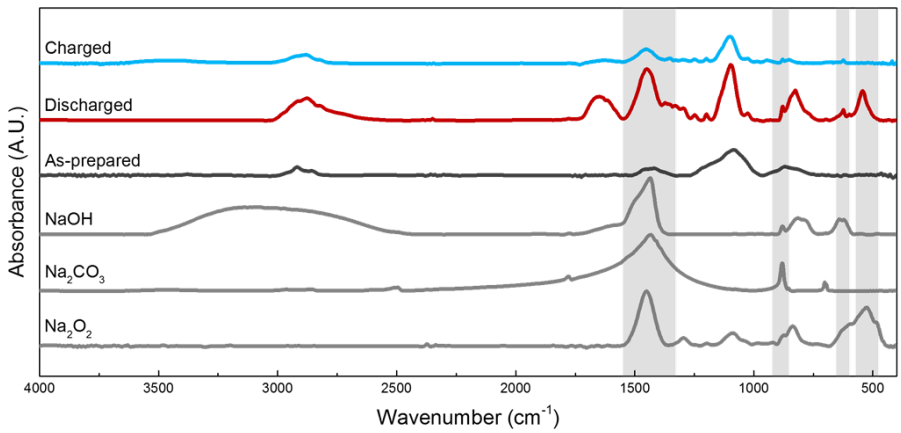

Figure 2–12. FTIR spectra after the initial discharge until the 1.8 V cut–off limit and the subsequent recharging processes with TEGDME electrolyte.

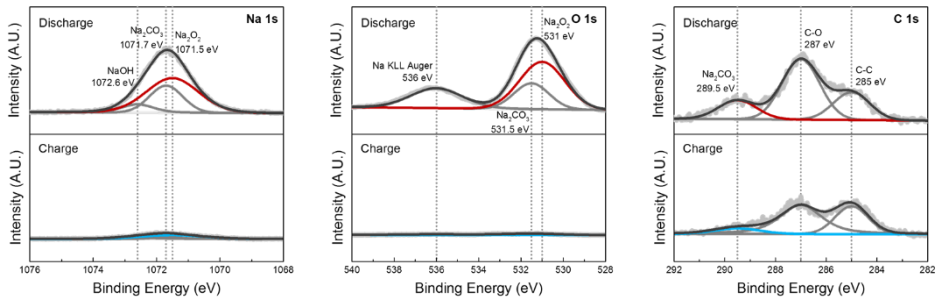

Figure 2–13. XPS measurements after the initial discharge until the 1.8 V cut–off limit and the subsequent recharging processes with TEGDME electrolyte.

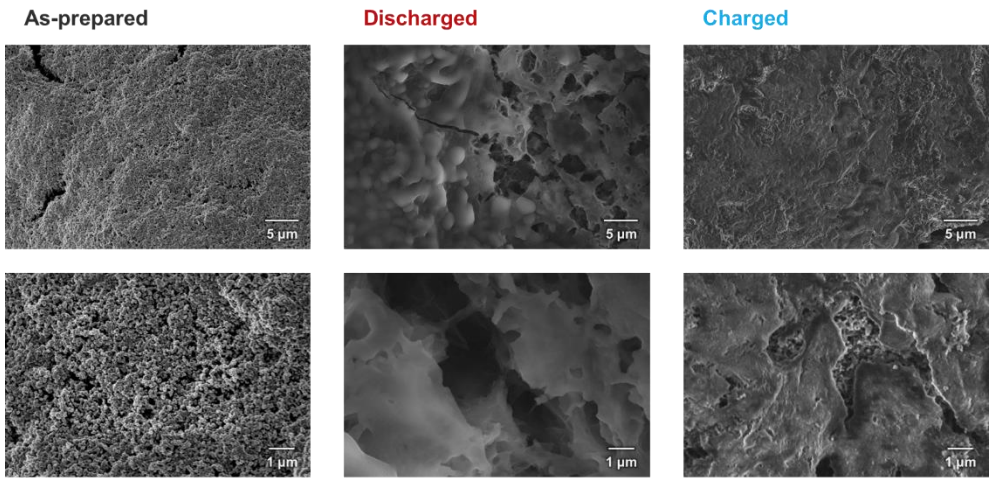

Figure 2–14. SEM images after the initial discharge until the 1.8 V cut–off limit and the subsequent recharging processes with TEGDME electrolyte.

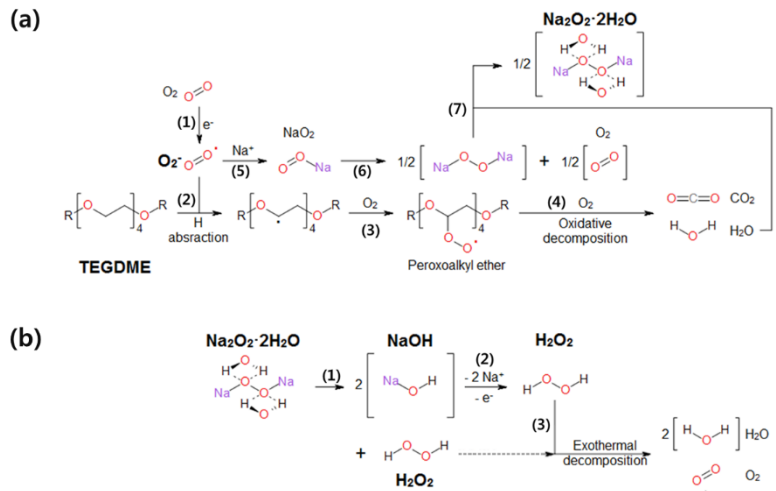

Figure 2–15. Schematic diagram of the proposed mechanisms for the (a) discharging and (b) charging processes with TEGDME electrolyte.

2.4 Conclusion

Sodium–oxygen batteries were investigated as an alternative to lithium–oxygen batteries in both carbonate and non–carbonate electrolyte systems. The sodium–oxygen cells could deliver high capacities, comparable to that of lithium–oxygen batteries but at slightly lower voltage. The charge and discharge mechanisms in sodium–oxygen cells were different and depended on the type of electrolyte. While the use of the carbonate based electrolyte resulted in cycling that was based on the formation and decomposition of sodium carbonate, the cell based on the non–carbonate electrolyte operated via the formation and decomposition of hydrated sodium peroxides. We proposed reaction mechanisms for the sodium–oxygen batteries based on the results reported here. Although the voltage of the sodium–oxygen battery is slightly lower than that of the lithium–oxygen battery, the abundance and economic merits of sodium make the sodium–oxygen battery a possible alternative to the lithium–oxygen battery.

2.5 References

1. Abraham, K.M. and Z. Jiang, *A polymer electrolyte–based rechargeable lithium/oxygen battery.* Journal of the Electrochemical Society, 1996. **143**(1): p. 1–5.

2. Bruce, P.G., *et al.*, *Li–O_2 and Li–S batteries with high energy storage.* Nature Materials, 2012. **11**(1): p. 19–29.

3. Freunberger, S.A., *et al.*, *Reactions in the rechargeable lithium–O_2 battery with alkyl carbonate electrolytes.* Journal of the American Chemical Society, 2011. **133**(20): p. 8040–8047.

4. Freunberger, S.A., *et al.*, *The lithium–oxygen battery with ether–based electrolytes.* Angewandte Chemie – International Edition, 2011. **50**(37): p. 8609–8613.

5. Black, R., *et al.*, *Screening for superoxide reactivity in Li–O_2 batteries: Effect on Li_2O_2/LiOH crystallization.* Journal of the American Chemical Society, 2012. **134**(6): p. 2902–2905.

6. Lim, H.D., *et al.*, *The potential for long–term operation of a lithium–oxygen battery using a non–carbonate–based electrolyte.* Chemical Communications, 2012. **48**: p. 8374–8376.

7. Lim, H.D., *et al.*, *Enhanced Power and Rechargeability of a Li−O_2 Battery Based on a Hierarchical–Fibril CNT Electrode.* Advanced Materials, 2012.

8. Lim, H.D., *et al.*, *Mechanism of Co_3O_4/graphene catalytic activity in Li–O_2 batteries using carbonate based electrolytes.* Electrochimica Acta, 2013. **90**: p. 63–70.

9. Kim, S.W., *et al.*, *Electrode Materials for Rechargeable Sodium-Ion Batteries: Potential Alternatives to Current Lithium-Ion Batteries.* Advanced Energy Materials, 2012. **2**(7): p. 710–721.

10. Website. *http://www.nistep.go.jp/achiev/ftx/eng/stfc/stt039e/qr39pdf/STTqr3904.pdf*. 2012.

11. Website. *http://www.che.ncsu.edu/ILEET/phevs/lithium–availability/An_Abundance_of_Lithium.pdf*. 2012.

12. Ellis, B.L. and L.F. Nazar, *Sodium and sodium–ion energy storage batteries*, in *Current Opinion in Solid State and Materials Science*2012.

13. Yabuuchi, N., *et al.*, *P2–type $Na_x[Fe_{1/2}Mn_{1/2}]O_2$ made from earth–abundant elements for rechargeable Na batteries.* Nature Materials, 2012. **11**(6): p. 512–517.

14. Peled, E., *et al.*, *Parameter analysis of a practical lithium– and sodium–air electric vehicle battery.* Journal of Power Sources, 2011. **196**(16): p. 6835–6840.

15. Sun, Q., Y. Yang, and Z.W. Fu, *Electrochemical properties of room temperature sodium–air batteries with non–aqueous electrolyte.* Electrochemistry Communications, 2012. **16**(1): p. 22–25.

16. Hartmann, P., *et al.*, *A rechargeable room–temperature sodium superoxide (NaO_2) battery.* Nature Materials, 2012. **12**(3): p. 228–232.

17. Chen, Y., *et al.*, *Li–O_2 battery with a dimethylformamide electrolyte.* Journal of the American Chemical Society, 2012. **134**(18): p. 7952–7957.

18. McCloskey, B.D., *et al.*, *On the efficacy of electrocatalysis in nonaqueous Li–O_2 batteries.* Journal of the American Chemical Society, 2011. **133**(45): p. 18038–18041.

19. Xu, W., *et al.*, *Investigation on the charging process of Li_2O_2–based air electrodes in Li–O_2 batteries with organic carbonate electrolytes.* Journal of Power Sources, 2011. **196**(8): p. 3894–3899.

20. Gallant, B.M., *et al.*, *Chemical and morphological changes of Li–O_2 battery electrodes upon cycling.* Journal of Physical Chemistry C, 2012. **116**(39): p. 20800–20805.

21. Ponrouch, A., *et al.*, *Non–aqueous electrolytes for sodium–ion batteries.* Journal of Materials Chemistry A, 2015. **3**(1): p. 22–42.

22. Srivastava, A.K. and R.A. Samant, *Ionic conductivity in binary solvent mixtures. 1. Propylene carbonate (20 mass %) + ethylene carbonate at 25°C.* Journal of Chemical and Engineering Data, 1994. **39**(2): p. 358–360.

23. Xu, K., *Nonaqueous liquid electrolytes for lithium–based rechargeable batteries.* Chemical Reviews, 2004. **104**(10): p. 4303–4417.

24. Lago, A., *et al., Study of static permittivity and density of the systems {(n–nonane + monoglyme or diglyme)} at various temperatures.* Journal of Chemical Thermodynamics, 2009. **41**(2): p. 257–264.

25. Riadigos, C.F., *et al., Permittivity and density of the systems (monoglyme, diglyme, triglyme, or tetraglyme + n–heptane) at several temperatures.* Journal of Chemical Thermodynamics, 2011. **43**(3): p. 275–283.

26. Hayamizu, K., *et al.*, *Pulse–gradient spin–echo 1H, 7Li, and 19F NMR diffusion and ionic conductivity measurements of 14 organic electrolytes containing LiN(SO2CF3)2.* Journal of Physical Chemistry B, 1999. **103**(3): p. 519–524.

27. Baysinger, G., *CRC Handbook of Chemistry and Physics*2012: Rensselaer Polytechnic Institute.

28. Doe, R.E., *et al.*, *First–principles investigation of the Li–Fe–F phase diagram and equilibrium and nonequilibrium conversion reactions of iron fluorides with lithium.* Chemistry of Materials, 2008. **20**(16): p. 5274–5283.

29. Brooker, M.H. and J.B. Bates, *Raman and infrared spectral studies of anhydrous Li_2CO_3 and Na_2CO_3.* The Journal of Chemical Physics, 1971. **54**(11): p. 4775–4787.

30. Moulder, J.F., *et al.*, Handbook of X–ray Photoelectron Spectroscopy, 1992.

31. Bryantsev, V.S. and M. Blanco, *Computational Study of the Mechanisms of Superoxide–Induced Decomposition of Organic Carbonate–Based Electrolytes*. Journal of Physical Chemistry Letters, 2011. **2**: p. 379–383.

32. Atkinson, R. and W.P.L. Carter, *Reactions of alkoxy radicals under atmospheric conditions: The relative importance of decomposition versus reaction with O_2*. Journal of Atmospheric Chemistry, 1991. **13**(2): p. 195–210.

33. Curran, H.J., *et al.*, *Oxidation of automotive primary reference fuels at elevated pressures.* Symposium (International) on Combustion, 1998. **1**: p. 379–387.

34. Wadhawan, J.D., *et al.*, *Microelectrode studies of the reaction of superoxide with carbon dioxide in dimethyl sulfoxide.* Journal of Physical Chemistry B, 2001. **105**(43): p. 10659–10668.

35. Roberts Jr, J.L., T.S. Calderwood, and D.T. Sawyer, *Nucleophilic oxygenation of carbon dioxide by superoxide ion in aprotic media to form the $C_2O_6^{2-}$ species.* Journal of the American Chemical Society, 1984. **106**(17): p. 4667–4670.

36. Xu, D., *et al., Novel DMSO–based electrolyte for high performance rechargeable Li–O_2 batteries.* Chemical Communications, 2012. **48**(55): p. 6948–6950.

37. Jung, H.G., *et al., A Transmission Electron Microscopy study of the electrochemical process of lithium–oxygen cells.* Nano Letters, 2012. **12**(8): p. 4333–4335.

38. Steiner, N. and W. Eul, *Peroxides and Peroxide Compounds, Inorganic Peroxides*. Kirk–Othmer Encyclopedia of Chemical Technology. Vol. 18. 2001: John Wiley & Sons, Inc.

39. Hwang, C.C., *et al., Bonding nature between oxygen and sodium on Si(113) surface.* Journal of Vacuum Science and Technology A: Vacuum, Surfaces and Films, 1998. **16**(3): p. 1073–1077.

40. Firsova, T.P., *et al.*, *Preparation and properties of sodium peroxide dihydrate* $Na_2O_2 \cdot 2H_2O$. Bulletin of the Academy of Sciences, USSR Division of Chemical Science, 1967. **15**(4): p. 724–726.

41. Beck, H.P. and G. Lederer, *High pressure transformations of NaOH.* Journal of Chemical Physics, 1993. **98**(9): p. 7289–7294.

42. Steiner, N. and W. Eul, *Peroxides and Peroxide Compounds, Inorganic Peroxides.* Kirk–Othmer Encyclopedia of Chemical Technology, 2001. **18**.

43. Chase, M.W., *NIST–JANAF Thermochemical Tables, 4th edition*. Journal of Physical and Chemical Reference Data, Monograph No. 9. Vol. 2. 1998: Americal Insititute of Physics.

44. Petigara, B.R., N.V. Blough, and A.C. Mignerey, *Mechanisms of hydrogen peroxide decomposition in soils.* Environmental science & technology, 2002. **36**(4): p. 639–645.

45. Beschkov, V., *et al.*, *Degradation of triethylene glycol dimethyl ether by ozonation combined with UV irradiation or hydrogen peroxide addition.* Water science and technology, 1997. **36**(2): p. 131–138.

Chapter 3. Dissolution and Ionization of NaO_2 in Sodium–Oxygen Batteries

(The content of this chapter has been submitted and being reviewed in *Nature Communications*. Reprinted with permission from [J. Kim *et al.*, *Nat. Commun.*, in revision (2015)].)

3.1 Introduction

To address the increasing use of renewable energy and launch of electric vehicles, the need for rechargeable batteries with high energy densities has been growing more rapidly than ever before.[1, 2] Among the available battery chemistries, metal–oxygen systems offer the highest energy density with the largest theoretical capacities. Unlike conventional lithium–ion batteries (LIBs), the direct reaction between oxygen and light metals such as lithium and sodium in metal–oxygen systems circumvents the need for a heavy transition metal redox couple in their operation, thereby making a high gravimetric energy density achievable.[3–7] The most intensively studied metal–oxygen system to date is the lithium–oxygen ($Li–O_2$) battery, which

shares a similar lithium chemistry with LIBs. However, this system suffers from poor cycle stability and efficiency, which has retarded the feasibility of its use in practical systems.[8, 9] In particular, the large charge overpotential over 1 V, the main reason for the low efficiency, also accelerates the degradation of the electrode and electrolyte.[9] As an alternative, Na has been introduced to replace Li in Li–O_2 batteries with a few important merits.[10] Despite the reduction of the energy density resulting from the lower redox potential of Na/Na^+, Na resources are readily available, less expensive than Li, and can easily replace Li in the battery chemistry. It has been reported that the redox reactions in the Na–O_2 battery result in an extremely low charge overpotential (~0.2 V) despite involving the formation of micrometer–sized sodium superoxide (NaO_2) cubic crystallites.[11–14] This unique phenomenon supports the idea that this system is a promising alternative not only in terms of the cost of materials but also regarding the potential practical performance advantages.

Notably, however, the reactions of Na–O_2 cells appear to be more diverse than those of Li–O_2 cells. Contrary to the initial report of NaO_2 discharge products, some recent works could not reproduce either the formation of the

discharge product NaO_2 or the low charge overpotential.[15–17] It was reported that sodium peroxide (Na_2O_2) [15–17] or sodium peroxide dihydrate ($Na_2O_2 \cdot 2H_2O$)[18, 19] were formed instead. In addition, these cells exhibited high overpotential during charge, similar to that observed in the Li–O_2 system. Many groups have attempted to determine the reasons for these discrepancies; however, to date, the main cause of the divergence of reactions has not been identified. Janek *et al.* investigated the effect of different carbon electrodes; Guo *et al.* and Shao–Horn *et al.* addressed this issue but observed no critical differences among the cases.[12, 20, 21]

In this work, we demonstrate the interplay of the diverse reactions in Na–O_2 batteries involving a series of electrochemical and chemical reactions as a function of time. Under systematic control of the operating conditions, we observe that the galvanostatic charge/discharge profiles are sensitively affected by the conditions and durations of the electrochemical operations. It is also revealed that the electrochemically formed NaO_2 is unstable and degrades into $Na_2O_2 \cdot 2H_2O$ in the absence of an applied current. The spontaneous dissolution and ionization of NaO_2 liberates the free O_2^- in the electrolyte and promotes side reactions involving the formation of

$Na_2O_2 \cdot 2H_2O$. Based on these observations, we propose reaction mechanisms of Na–O_2 batteries under various operating conditions. This report is the first to reveal the relationships among the different discharge products observed in Na–O_2 batteries, which broadens our understanding of the electrochemical and chemical reactions in Na–O_2 batteries. Furthermore, these discussions may offer insight and guidance to the metal–air battery community in terms of regulating the kinetics of the intertwined reactions.

3.2 Experimental

3.2.1 Cell assembly and galvanostatic cycling of Na–O_2 cells

The carbon cathode was prepared by casting Ketjen Black carbon paste and polytetrafluoroethylene (PTFE) (60 wt% emersion in water, Sigma–Aldrich) with a mass ratio of 9:1 in a solution of isopropanol (IPA: >99.7%, Sigma–Aldrich) and N–methyl–2–pyrrolidone (NMP: 99.5%, anhydrous, Sigma–Aldrich) with a volume ratio of 1:1 on Ni mesh current collectors. The carbon–coated Ni mesh was dried at 120 ℃ and heated at 400 ℃ for 4 h in Ar to completely remove any residual H_2O impurities.

All the procedures described below were performed in an Ar–filled glove box (O_2 level < 0.5 ppm, H_2O level < 0.5 ppm). The Na–O_2 cells were assembled as a Swagelok–type cell with stacking of the Na metal anode, electrolyte–soaked separators, and carbon cathode, which was punched with a ½ –inch diameter. The Na metal anode was carefully prepared by milling dry Na metal chunks (ACS Reagent, Sigma–Aldrich) after removing the contaminated surfaces. The electrolyte was prepared with diethylene glycol dimethyl ether (DEGDME, anhydrous, 99.5%, Sigma–Aldrich), which

contains 0.5 M $NaCF_3SO_3$ (98%, Sigma–Aldrich). The solvent was dried using 3–Å molecular sieves for over one week, and the salt was also kept in a vacuum oven at 180 ℃ for the same time before use. The final water content in the electrolyte was less than 10 ppm according to a Karl–Fisher titration measurement. The amount of electrolyte used for the cell was 200 μL. Two sheets of Celgard 2400 were used as separators. Electrochemical battery tests of the Na–O_2 cells were conducted using a potentio–galvanostat (WonA Tech, WBCS 3000, Korea). All the cells were relaxed under 770 torr of O_2 pressure for 10 min before the tests. After being saturated with O_2 gas, the cells were operated in the closed state with a limited capacity of 1 mAh, lower voltage cutoff of 1.6 V, and upper voltage cutoff of 4.2 V.

Special protocol based on a pulsed current was applied during the charge to avoid dendritic failure of the Na metal anode. The on/off time ratio of the pulse charge was 1:4 (applying current for 0.5 s and relaxing for 2 s). More details about our charge protocol are provided in Figure 3–2. In our galvanostatic cycling experiments of Na–O_2 cells, the dendritic failure of the Na metal anode was frequently observed during the charge process, similar to previous reports. The SEM images of the separators collected after cycling

with the direct currents are presented in Figure 3–2a–c, which reveal that the Na metal clogged and penetrated the pores of the separators, resulting in the dendritic growth of the Na metal and failure of the cells. The Na dendrites were visually inspected, as shown in the photographs of the separators and anodes in Figure 3–2g. These dendrites were critically damaged during the cycling process, resulting in short circuits and potential failures. To suppress and avoid the dendritic growth of Na metal, we applied special operating protocols based on pulse–charging, which is a common methodology in electroplating and deposition. Several researchers in the battery community have already reported on pulse–charging to suppress the dendritic growth of Li metal. Under these conditions, the stable electrochemical cycling of Na–O_2 cells without any voltage fluctuations or sudden drops was possible. The SEM images in Figure 3–2d–f also demonstrate the absence of dendritic Na metal penetrating or clogging the pores of the separators. In addition, the upper surface of the pulse–charged Na metal in Figure 3–2i is seemingly much cleaner than that of the direct–current–charged Na metal. Meanwhile, it was concerned that the rest time between the inter–current periods could affect our experimental observations, because one of the main key parameters

for regulating the electrochemical and chemical reaction was the rest time between the discharge/charge. However, as shown in Figure 3–4, we found that the inserted resting as a pulse did not have any effect on the experimental responses. This strongly indicated that the continuously accumulated resting time during the electrochemical operation was only meaningful.

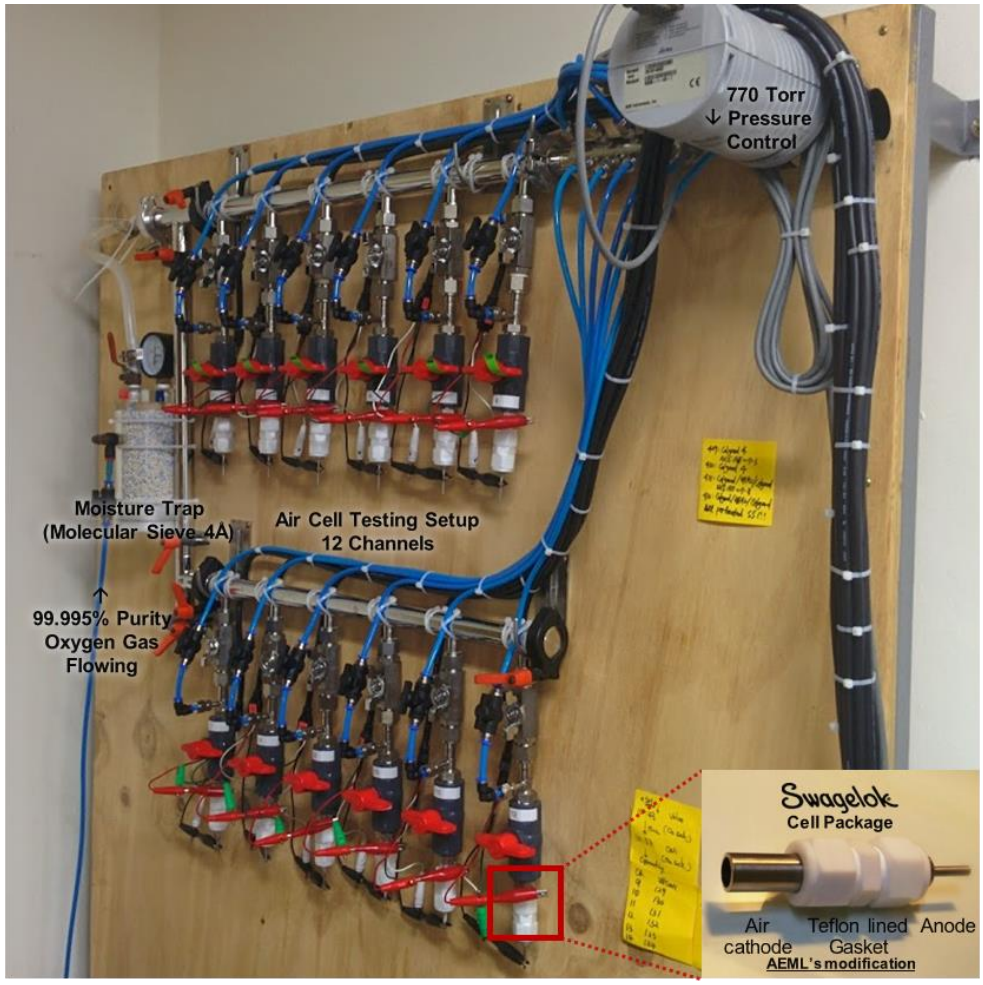

Figure 3–1. Modified experimental setup installing independent serial 12−channel for galvanostatic cycling of Na–O_2 batteries. Inset represents the detailed figure of Swagelok–type cell.

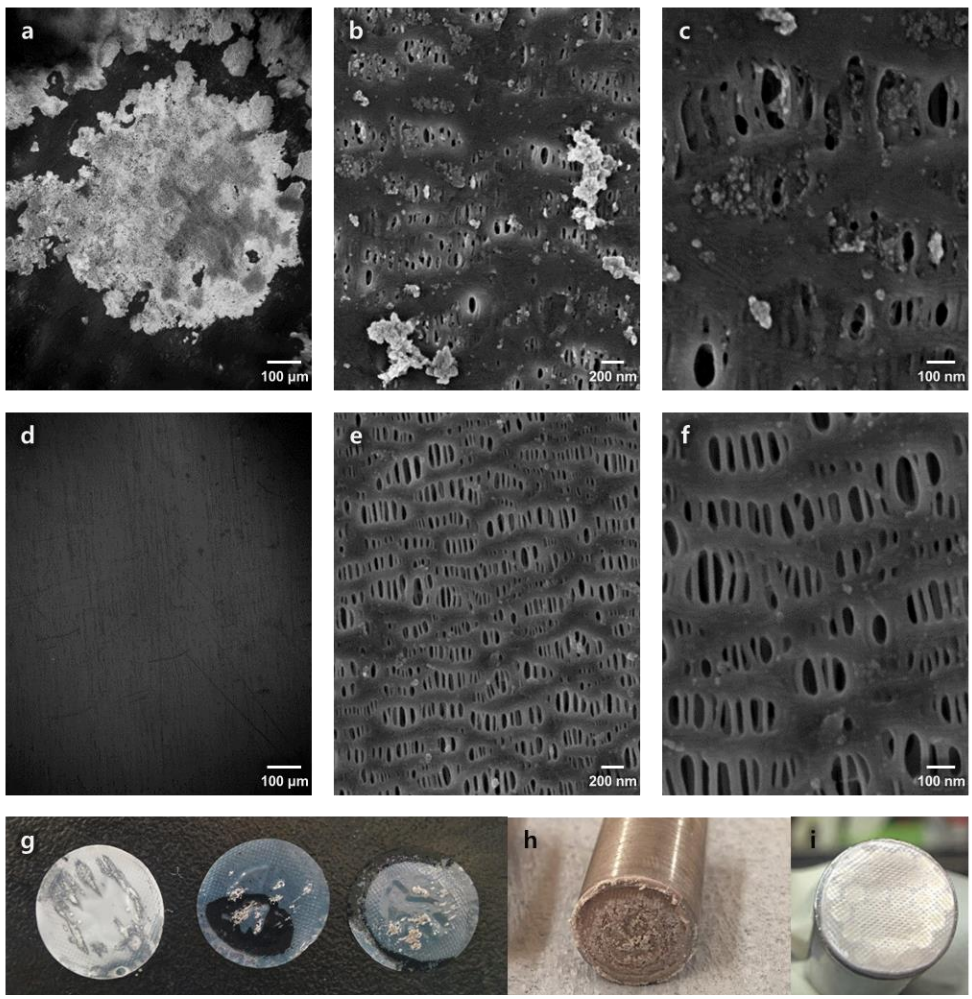

Figure 3–2. SEM images and photographs of Na dendrites after the cycling of Na–O_2 cells. (a)–(c) SEM images of Na dendrites after the cycling of Na–O_2 cells using direct currents; (d)–(f), pulse currents during the charge process. (g) Photographs of Na dendrites on the separators after cycling; (h) Na anode with the direct current. (i), surface of Na anode for the pulsed current.

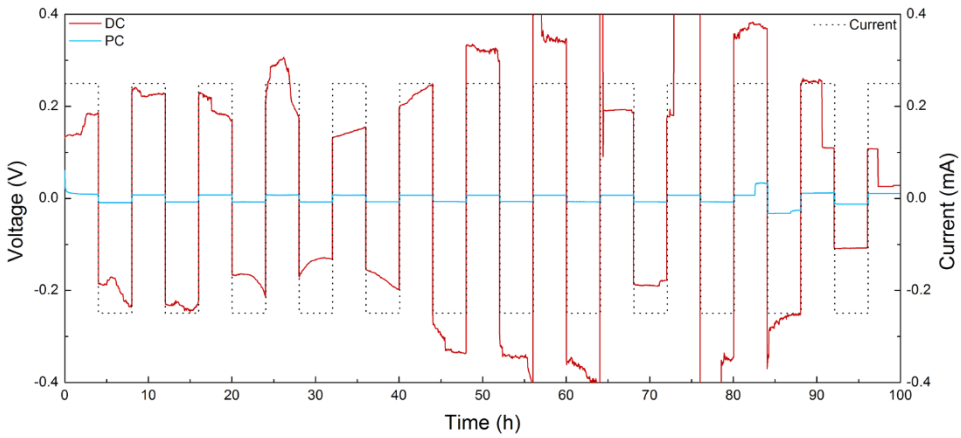

Figure 3–3. Voltage profiles of symmetric cells (Na / electrolyte / Na) in constant current (Red : direct current, PC : pulsed current).

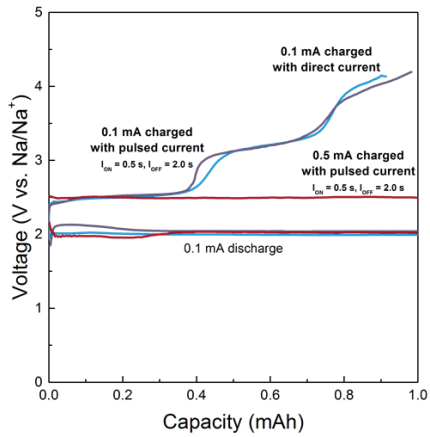

Figure 3–4. Electrochemical characteristics of Na–O_2 cells charged with direct current, pulsed current, and averaged current including the pulsed rest time.

3.2.2 Characterization of Na–O_2 cells

The discharged cathodes after the different rest times were collected from disassembled Na–O_2 cells and washed with acetonitrile (anhydrous, 99.8%, Sigma–Aldrich) in a glove box to remove any residual electrolyte. X–ray diffraction (XRD) spectra of the cathodes were obtained using a Bruker D2–Phaser (Cu Kα λ=1.5406 Å) with the aid of a specially designed air–tight holder to prevent outer atmospheric contamination. Raman spectra were obtained using a Horiba Jobin–Yvon LabRam Aramis spectrometer (the 514 nm line of an Ar–ion laser was used as the excitation source). The scattered light of the Raman signal was collected in a backscattering geometry using the x50 microscope objective lens. Field–emission scanning electron microscopy (FE–SEM, MERLIN Compact, ZEISS, Germany) was used for the morphological observations after Pt coating. For electron spin resonance (ESR) characterization, the collected powder from the discharged cathodes after rinsing to remove the residual used electrolytes was soaked in fresh electrolyte. After immersing the powdery discharged cathodes, the ESR signal of the electrolytes was measured at room temperature using a JEOL

JES–TE200 ESR spectrometer every 10 min for 12 h using a liquid quartz–cell. The microwave X–band frequency was 9.42 GHz at 1–mW power.

3.2.3 Theoretical calculations of solvation energy

First–principles calculations were performed using the spin–polarized generalized gradient approximation (GGA). A continuum solvation model (VASPsol[22, 23] code) was used to evaluate the solvation energy of the alkali–metal superoxide/peroxide (M_xO_2, M: Li, Na, x = 1 or 2). The following equations were used considering both the (1) molecular and (2) ionized solvated states:

$$\Delta E_{\text{sol, mol}} = E_{\text{solvated}}(M_xO_2) - E_{\text{bulk}}(M_xO_2) \quad (1)$$

$$\Delta E_{\text{sol, ion}} = x \cdot E_{\text{solvated}}\left(M^{+}\right) + E_{\text{solvated}}(O_2{}^{x-}) - E_{\text{bulk}}(M_xO_2) \quad (2)$$

where $E_{\text{solvated}}(M_xO_2)$ and $E_{\text{bulk}}(M_xO_2)$ are the total energies of the solvated and bulk M_xO_2 per formula unit, respectively. The solvated species (ions or molecules) were placed in a 13 Å × 13 Å × 13 Å cell as an isolated species. We used the plane–wave basis with an energy cut–off of 550 eV and a Monkhorst–Pack 2×2×2 *k*–point mesh. Based on previous reports[24, 25] that stated that the solvation entropy term (TS) of polar molecules and ions in the standard state is less than 5% of the enthalpy term (H), we neglected the entropy effect of the solvation in these calculations.

3.3 Results and Discussion

3.3.1 Dependency of galvanostatic charge/discharge profile on the operating conditions

To address the previous conflicting results on the discharge products and overpotentials of Na–O_2 cells, we carefully assessed the effects of operating parameters on the resulting electrochemical profiles. Among the various parameters examined (Figure 3–5–Figure 3–8), we observed that the charge/discharge profiles were most sensitively affected by the applied current and rest time between the discharge and charge, which was analogous to the report by Yadegari *et al*. as a function of discharge current or limited capacities[19]. Figure 3–5 presents and compares the electrochemical profiles obtained under various conditions. Although the discharge profiles are similar, with a single plateau at ~2.1 V, there are roughly three different charging plateaus observed at (i) ~2.5 V, (ii) ~3.0 V, and (iii) 3.8 V, which agree with recent reports under certain settings.[19, 20] However, the relative lengths of each plateau markedly vary under differing operating conditions. For the cases of controlled discharge currents followed by a constant current charging in Figure 3–5a, it was observed that the length of the lower plateau (~2.5 V)

in the charge profiles was reduced as the applied discharge current decreased from 0.5 to 0.02 mA. However, the lengths of the plateaus at higher voltages, *i.e.*, ~3.0 and 3.8 V, were substantially increased, resulting in an overall larger overpotential. Similar behaviors were observed in Figure 3–5b when varying the charge currents after a constant current discharge. With the lower applied charge currents, the cell exhibited a higher charging overpotential with shortened plateau length at 2.5 V. This result contrasts with the general observation that slow charging/discharging of electrochemical cells results in a voltage close to the equilibrium potential, thereby resulting in smaller overpotentials. In addition, this result strongly indicates that the different discharge products might undergo the charging process at each case. Notably, the shapes of the electrochemical charge profiles provide important clues to determine the discharge products of Na–O_2 reactions.[19, 26] Even though the discharge products should be identical for the cases of the same protocol of discharge, each charge profile was distinct with different charge currents. This finding implies that the initial discharge products are gradually transformed into other phases during the charge process *via* time–dependent reactions. To verify whether this transformation occurs *via* an electrochemical

or chemical reaction, we also controlled the rest time between the discharge and charge processes. As observed in Figure 3–5c, the lowest voltage region in the charge profiles systematically decreases upon increasing the rest time from 0 to 12 h. The change in the electrochemical profile in the absence of the applied current clearly indicates that the time–dependent chemical reactions occurred during the rest period, affecting the subsequent charging.

The time–dependent chemical reactions can be more clearly visualized by plotting all the voltage profiles as a function of the time. Figure 3–5d–j illustrate the voltage evolution of each cell after the completion of the discharge at different operating conditions. The first inflection points of the voltage profiles at charge (indicated with arrows) occur at approximately 10 h regardless of the rest or charge protocols. This result indicates that a specific time of ~10 h is required before observing a change of the profile, which hints at the kinetics of the chemical reactions.

Similar behavior was also confirmed in similar tests for the higher charging currents with the resting time after the discharge, which revealed the growth of the charge polarizations upon increasing the rest time (Figure 3–6). The

introduction of the rest time between the discharge/charge enables us to assess the effects of a non–electrochemical process on the voltage profiles, as discussed in the main discussion section. Even the high charge currents without any rest resulted in low polarization of charge; the insertion of rest time led to an increase in the charge polarizations. Thus, the effects of the chemical reactions were reconfirmed by similar electrochemical tests with relatively high charge currents. Moreover, the voltage after the 24–h rest has no flat region at 2.4 V, which is closely related to the decomposition reaction of NaO_2.

We determined that the charge behaviors of Na–O_2 cells could be altered by the utilized capacities even with equally applied currents, as demonstrated in Figure 3–7. Unlike the capacity–limited cycling, the voltage profile without any capacity limit shows a low polarized charge potential over the entire capacity range, as observed in Figure 3–7b. This finding indicates that the NaO_2 formed without limited capacity was relatively stable and could be electrochemically decomposed rather than chemically deformed. Even though further analyses might be required to attain a clear understanding, we believe that the size of the discharged crystallite is also importantly affected

by the dissolution of NaO_2. Thus, the longer lifetime of the large–sized NaO_2 from the fully operated discharge was attributed to the slow kinetics of dissolution in the electrolytes resulting from its low interfacial surface–to–volume ratio.

We also investigated the cycle properties of Na–O_2 cells depending on the shape of the charge profiles by simply controlling the charge currents. Figure 3–8 demonstrates the better reversibility achieved with the low charge potential compared with the highly polarized charge profile. The irreversible reactions with the lower charge current might be due to the chemical evolution of $Na_2O_2 \cdot 2H_2O$, which shows the 3–step charge profile.

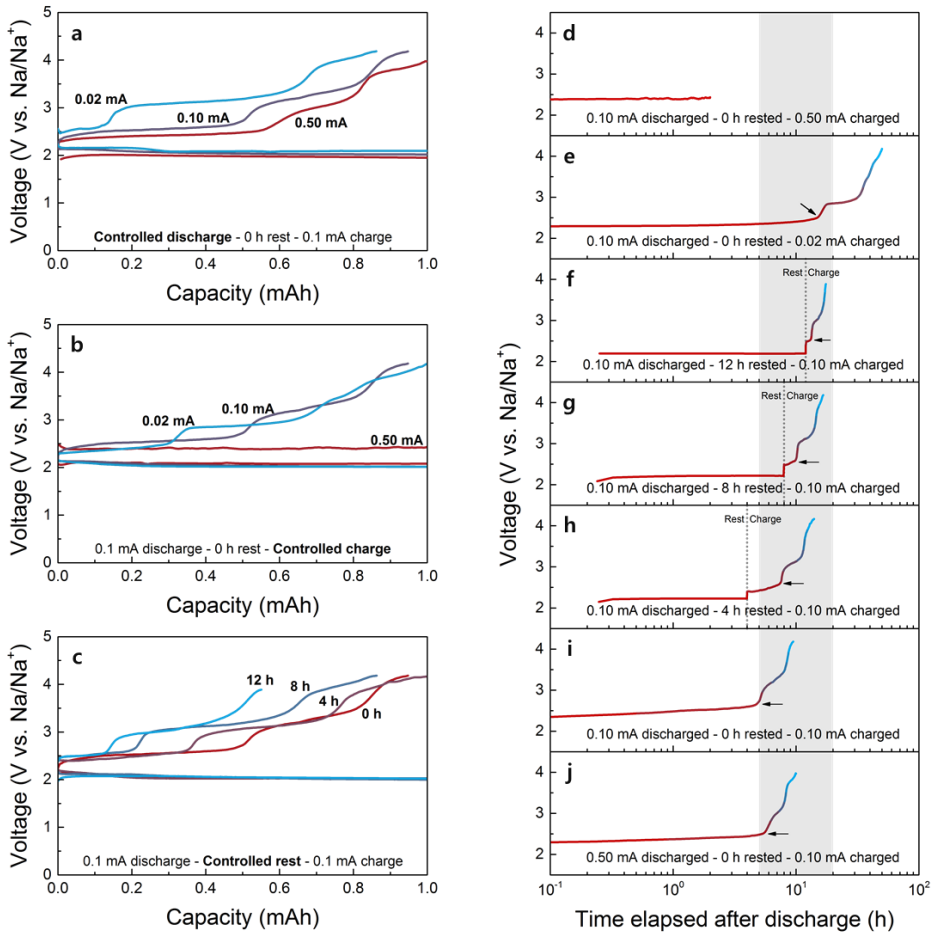

Figure 3–5. Electrochemical charge/discharge profiles of Na–O_2 cells under various operating conditions. (a) Discharge currents of 0.02, 0.1, and 0.5 mA; (b) charge currents of 0.02, 0.1, and 0.5 mA. All the cells utilized a limited capacity of 1.0 mAh; and (c) rest times of 0, 4, 8, and 12 h. (d)–(j), Representations of voltage profiles as a function of time corresponding to (a)–(c). The shaded area indicates that range of the first points of the polarized charge potentials

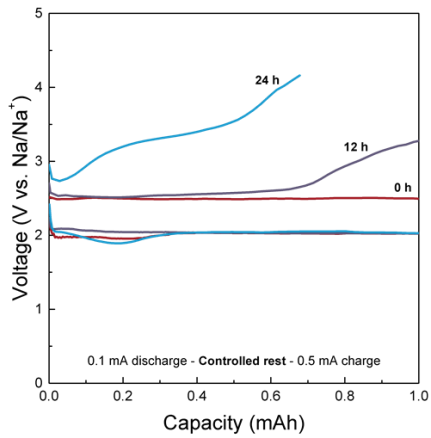

Figure 3–6. Electrochemical characteristics of Na–O_2 cells under high charge currents combined with rest time.

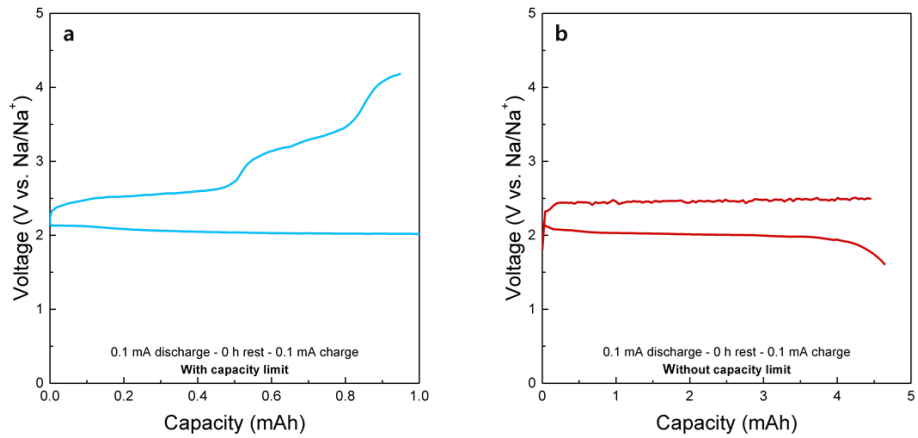

Figure 3–7. Electrochemical characteristics of Na–O_2 cells. (a) Operation of Na–O_2 cells with limited capacity of 1 mAh. (b) Full operation of Na–O_2 cells without the capacity limit. The applied currents were identical for both cells.

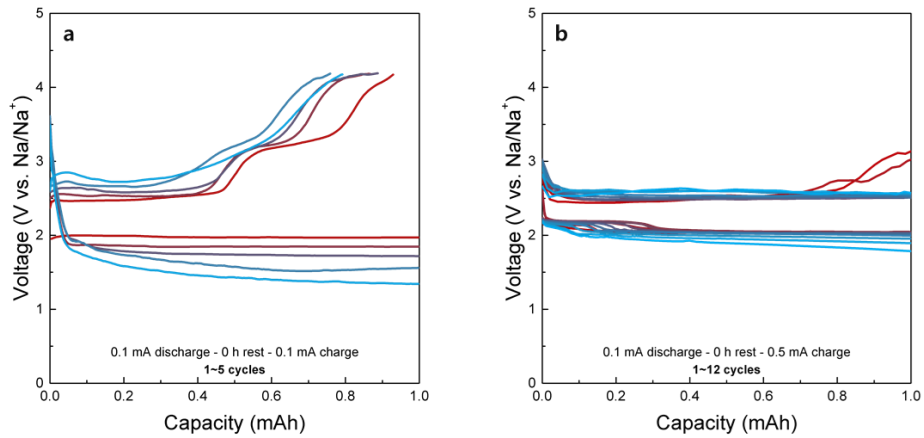

Figure 3–8. Electrochemical characteristics of Na–O_2 cells with the different voltage profiles over several cycles. (a) Cycling up to 5 cycles with a charge current of 0.1 mA involving clear 3–step charge profiles. (b) Cycling up to 12 cycles with the charge current of 0.5 mA involving the lower flat charge profiles.

3.3.2 Time–resolved characterization of discharge products

To confirm the time–dependent phase transformation of the discharge products *via* chemical reaction in Na–O_2 cells, we characterized the discharge products in air electrodes as a function of the rest time. The highly crystalline NaO_2 was observed directly after the discharge with no other phases, as demonstrated in the X–ray diffraction (XRD) spectra (Figure 3–9a–b).[11] However, after being aged for several hours, the NaO_2 peak slowly diminished, whereas the characteristic peak of $Na_2O_2 \cdot 2H_2O$ began to appear and grew. After 12 h of resting, the initial discharge product was completely transformed into $Na_2O_2 \cdot 2H_2O$. It should be noted that $Na_2O_2 \cdot 2H_2O$ has often been regarded as a main discharge product in previous reports of Na–O_2 batteries.[18–20] Recently, Ortiz–Vitoriano *et al*. reported that NaO_2 could convert to $Na_2O_2 \cdot 2H_2O$ upon exposure to the ambient air during the characterization at room temperature[21]. However, our data show that such transformation occurs in the electrochemical cells by the intrinsic dissolving characteristics of NaO_2 in the electrolyte even without the exposure to the ambient atmosphere. Remarkably, the time taken for the discharge product to completely transform into $Na_2O_2 \cdot 2H_2O$ coincides with the timeline of Figure

3–5d–j, which shows the inflection of the voltage rising after approximately 10 h. When we analyzed the phases of the discharge products as a function of the applied discharge currents (Figure 3–10), it was also observed that the $NaO_2/Na_2O_2 \cdot 2H_2O$ ratio decreased with the lower operating current, which is consistent with the time–dependent transformation of the discharge products.

Raman spectroscopy results confirmed that the initial NaO_2 discharge products gradually transformed into $Na_2O_2 \cdot 2H_2O$ with resting. In Figure 3–9c, the two distinct peaks of NaO_2 and $Na_2O_2 \cdot 2H_2O$ are detected along with the characteristic bands (D/G) of the carbon electrode. The Raman signals at 1156 and 1136 cm^{-1} are attributed to the O–O stretch bonding in NaO_2 and $Na_2O_2 \cdot 2H_2O$, respectively.[21] The systematic change in the relative ratios of NaO_2 and $Na_2O_2 \cdot 2H_2O$ with time is clearly illustrated in Figure 3–9d, which agrees well with the results in Figure 3–9b. The phase transition of NaO_2 to proton–containing $Na_2O_2 \cdot 2H_2O$ indicates a source of protons in the electrochemical cell. Considering the low water content in the electrolyte used for the cell (< ~5 ppm), which is insufficient to form the phase,[27] the protons are likely delivered from other sources such as the electrolyte solvent. As we could expect, the rechargeability of $Na–O_2$ cell was better for the

highly biased electrochemical conditions coupled with the low polarized charge profile which is attributed to the formation of NaO_2 as shown in Figure 3–8. However, the electrochemical reversibility with the 3–steped charge profile shown from $Na_2O_2 \cdot 2H_2O$ was relatively worse compared to the former conditions. The proposed transformation mechanism will be discussed in detail later.

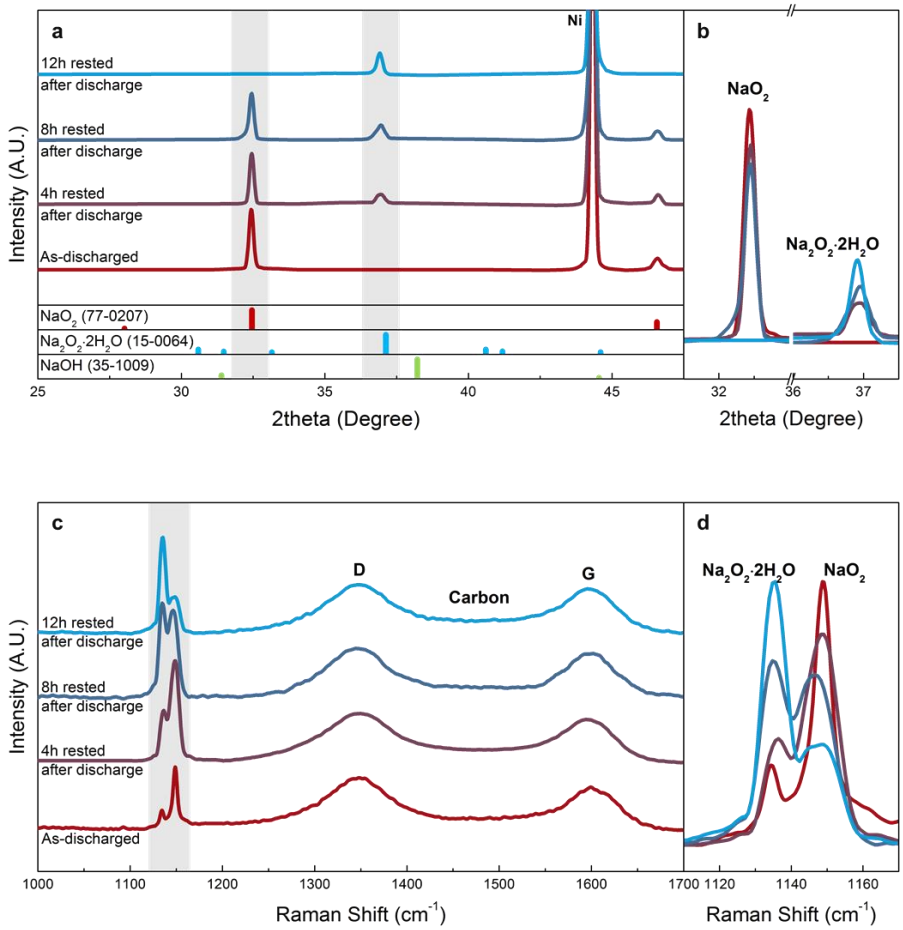

Figure 3–9. Time–resolved characterization showing the phase transitions of the discharge products of the Na–O_2 cells. (a), (b) XRD spectra of the discharged cathodes of Na–O_2 batteries with rest times of 0, 4, 8, and 12 h. (c), (d), Raman spectra of the discharged cathodes of Na–O_2 batteries with rest times of 0, 4, 8, and 12 h.

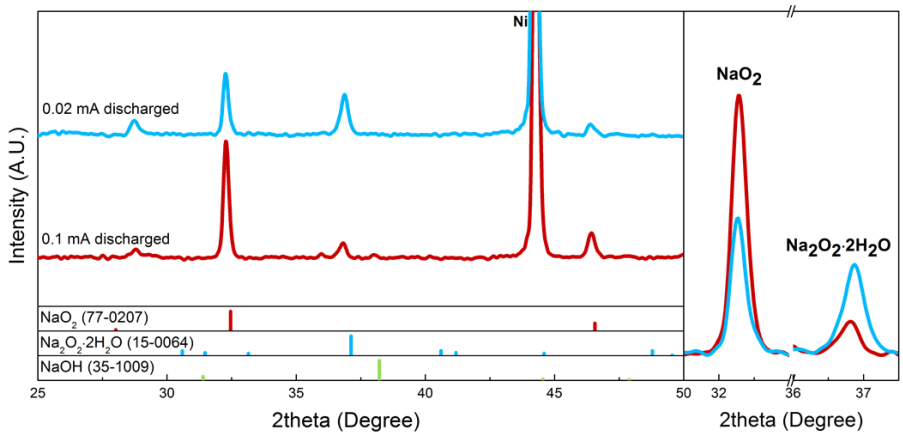

Figure 3–10. XRD spectra of the discharged cathodes of Na–O_2 cells for different discharge currents with the full discharge capacity of 4 mAh.

XRD analysis clearly demonstrates that a larger amount of NaO_2 transformed into $Na_2O_2{\cdot}2H_2O$ during the discharge at the relatively smaller current of 0.02 mA because of the longer time exposure to the electrolyte.

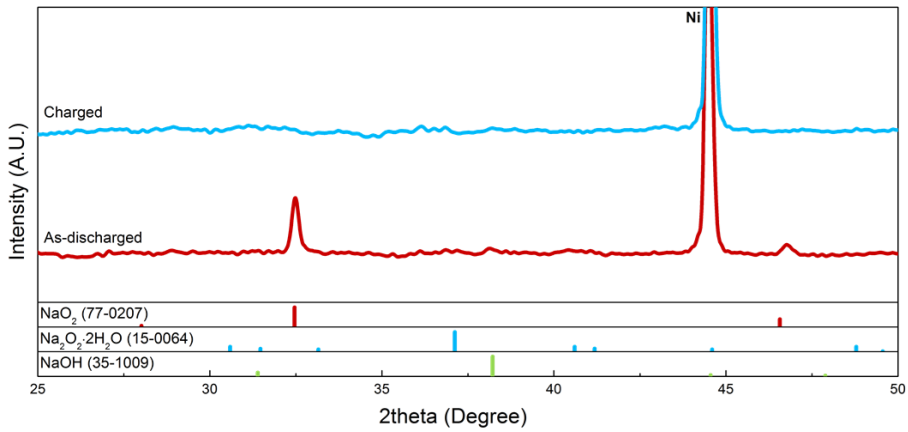

Figure 3–11. XRD analysis of the formation and decomposition of NaO_2 after the discharge and charge.

3.3.3 Morphological change of discharge products over time

To visualize the transition process, we examined the morphologies of the discharge products at different rest times within 12 h. In Figure 3–12a, well–defined micron–sized cubic NaO_2 was observed immediately after the discharge, which agrees with the observation of Hartmann *et al.*[11] However, the edges of the cubes became significantly dull, and the overall shapes of the cubes obtained were smudged during the rest period (Figure 3–12b–c). At the end of the rest period, the cubic crystallites completely disappeared, and rod–shaped microparticles began to appear, which resemble the $Na_2O_2 \cdot 2H_2O$ in a previous report.[19] This morphological change suggests the disappearance of NaO_2 and the subsequent appearance of $Na_2O_2 \cdot 2H_2O$ in the cell during the rest period. Moreover, this finding implies that the transformation does not occur *via* a conventional solid–state or interfacial reaction between NaO_2 and the electrolyte to form $Na_2O_2 \cdot 2H_2O$, which would not involve significant morphological change. Rather, it is likely to be a solution–mediated process through dissolution and nucleation.[28–30]

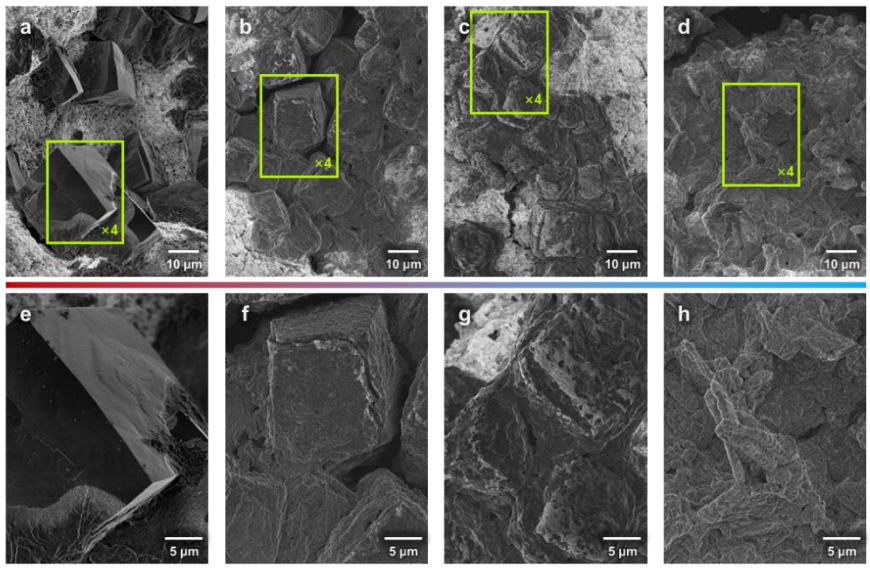

Figure 3–12. Time–resolved examinations of the morphology of discharge products on the cathodes of Na–O_2 cells. (a)–(d) Morphology of the discharge products of Na–O_2 cells. (e)–(h) Corresponding magnified SEM micrographs; (a), (e) as–discharged, (b), (f) 4–h rest after discharge, (c), (g) 8–h rest after discharge, and (d), (h) 12–h rest after discharge.

3.3.4 Dissolution and ionization of NaO_2

We investigated the possibility of the dissolution of the solid NaO_2 phase in the electrolyte using electron spin resonance (ESR) spectroscopy, which is useful for detecting the magnetic responses of the unpaired electrons in radicals such as O_2^-.[31] Surprisingly, as observed in Figure 3–13a, with the simple immersion of the pre–discharged cathodes, the ESR signal evolved within 10 min from the fresh electrolyte, indicating the presence of O_2^-. To avoid any effect of the remaining oxygen from the disassembled Na–O_2 cells, the pre–discharged cathodes were washed with fresh electrolyte before the measurement, which led to an identical result. The calculated *g*–value of 2.0023 for the observed ESR signal corresponds well with the theoretical value of the unpaired electron in free O_2^-[32]. The solubility of NaO_2 in the electrolyte was roughly estimated about 187 mM, which is in the similar order with the report by Schechter *et al*.[33], but has a relatively large discrepancy to the report by Hartmann *et al*[34]. This discrepancy might be mainly due to the additional chemical reactions involving the precipitation of solid $Na_2O_2 \cdot 2H_2O$. The detection of O_2^- indicates that the NaO_2 is soluble in the ether–based electrolytes, which was also expected from the literatures with

the electrochemical determinations[21, 34, 35]. Furthermore, this behavior is analogous to highly soluble LiO_2 in the solvatable conditions of Li–O_2 batteries[27, 36]. More importantly, the dissolution can immediately lead to the ionization of NaO_2, liberating O_2^-, the consequences of which will be discussed later.

Figure 3–13b shows that the peak–widths of the ESR signals increased slightly with time. The broadening indicates the energy exchange of the spin with the local environments *via* spin–spin relaxation or spin–lattice relaxation.[31] This interaction supports the time–dependent chemical reactions associated with the dissolved O_2^- with its neighboring electrolyte solvent. The intensity of the O_2^- signal is the highest approximately 20 min after the immersion and exponentially decreases over time, indicating the instability of O_2^- in the electrolyte.[37] From this behavior, we could derive that it was a pseudo–first order reaction which mainly relates with the concentration of O_2^-. Based on the exponential fitting of the relative intensity of ESR signals, the pseudo–first order rate constant of H^+–abstraction was obtained as about $k' \approx 0.560$, and its corresponding half–life was estimated as about $t_{1/2} = \ln(2) / k' \approx 1.24$ h. Figure 3–13c reveals, however, that the time–

dependent decay of the intensity is relatively sluggish compared with the intrinsic lifetime of normal O_2^-. Typically, the half–life of O_2^- is approximately 1–15 min because of its high reactivity and instability.[38] The abnormally long half–life in the electrolyte (~1.24 h) in our case is believed to occur because O_2^- is continuously generated with the dissolution of NaO_2. The ESR signal completely vanished after approximately 8 h, which is slightly faster than the time required for the formation of $Na_2O_2 \cdot 2H_2O$ in Figure 3–13. Despite the evolution of O_2^-, the overall signal decay might be induced from the relatively dominant H^+–abstraction due to the reactivity of O_2^-. This gap in the kinetics might originate from the time required to form the $Na_2O_2 \cdot 2H_2O$ phase from the O_2^-.

To understand the dissolution and ionization behavior of NaO_2, the solvation energies of various alkali metal superoxides and peroxides were calculated for comparison using first–principle calculations. Figure 3–13d reveals that generally, the superoxide exhibits a lower solvation energy than the peroxide for both lithium and sodium compounds. This result is consistent with our result of NaO_2 dissolution and the recent experimental findings for Li–O_2 batteries, which indicated that LiO_2 is found mostly as soluble

intermediates in the electrolyte in contrast to the solid phase of Li_2O_2. [27, 36] In addition, it is notable that the solvation energy of the sodium phases was significantly lower than that of the lithium phases, which is attributed to the weaker Lewis acidity of the Na cation compared with that of the Li cation in the polar solvent.[39, 40] However, for the solvents with substantially lower dielectric constant (ε = ~ 7), the dissolution does not significantly occur even in NaO_2. Molecular dissolution energies of NaO_2 in model solvents are ~0.6 eV, which roughly corresponds to 1 molecule dissolution out of 10^{10} formula unit of NaO_2. On the other hand, it remarkably decreases to 0.17 eV (1 molecule out of 1000 formula unit of NaO_2) in ε = 30. It is well known that for low dielectric constant solvents, the solution dielectric constant sensitively increases as the salt concentration increases, which can be well higher than that of the pure solvent[41]. Therefore, it is expected that the dissolution of NaO_2 can occur when salts are present in the electrolyte, which is consistent with the observation of O_2^- in the ESR analysis. It is noted that even with the dissolving characteristics of NaO_2, the crystallization of NaO_2 is possible in the normal discharging conditions with the supersaturation of localized reactants such as Na^+ and O_2^- [21, 34, 42, 43]. In the other case where the

supply of the reactants such as Na^+ are limited, for example, in the absence of the applied voltage, the dissolution and ionization might dominate giving rise to the formation of $Na_2O_2 \cdot 2H_2O$ as a discharge product.

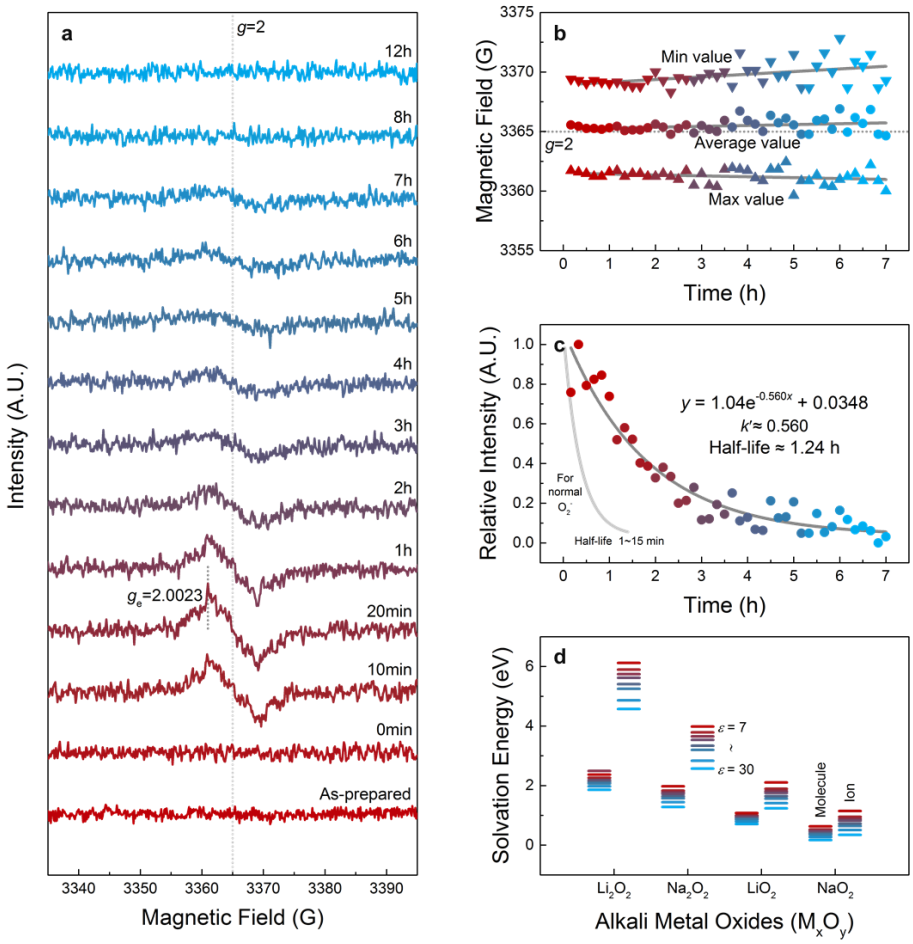

Figure 3–13. **ESR analysis and theoretical calculations of the dissolution and ionization of NaO_2 into the electrolyte.** (a) Time–dependent ESR measurements for the fresh electrolytes (0.5 M $NaCF_3SO_3$ in DEGDME) with soaking of the pre–discharged cathode without any aging. (b) Maximum, minimum, and average values of ESR signals as a function of time. (c) Exponential decay of ESR signals and the common trend line of O_2^-. (d) Calculations of the solvation energy for several alkali–metal superoxides and peroxides with the various dielectric constants (ε = 7~30).

3.3.5 Proposed mechanism of Na–O_2 batteries

Based on the previous reports and our new findings, we propose a mechanism that describes the electrochemical and chemical reactions in Na–O_2 systems in Figure 3–14. The well–established discharge process[11] can be illustrated with the reduction of an O_2 molecule into O_2^-, which reacts with Na^+ to form NaO_2 (Reaction 1), and the charge process is the reverse reaction (Reaction 2). After or during the discharge, the NaO_2 is prone to dissolution and ionization into the electrolyte based on the solvating energy (ΔG_{sol}) in the solvent (Reaction 3).[36] The dissolution of NaO_2 generates O_2^-, which can degrade the surrounding molecules because of its chemical instability. Typically, the liberated O_2^- is a strong reagent for the abstraction of H^+ from the electrolyte solvents (Reaction 4),[9] and the degree of H^+ abstraction[44, 45] is determined by the acid–dissociation constant (pK_a) of the solvent. Some hydroperoxyl radicals (HO_2) might be formed during this process, resulting in the nucleophilic attack of the H^+–lost solvent (Reaction 5)[46]. However, the evolution of HO_2 can be helpful to promote the solution–mediated discharge/charge process as recently reported by Xia *et al*.[35]. Nevertheless, in a circumstance where the dissolution/ionization of NaO_2 is dominant, the

liberation of O_2^- is overwhelmingly larger than a possible HO_2 formation inducing the H^+–abstraction from the neighboring electrolyte solvent. Meanwhile, the solvent undergoes oxidative decompositions to produce byproducts such as carbon dioxide (CO_2), water (H_2O), and hydroxyl anions (OH^-) (Reaction 6)[47]. It is also possible that the coupling of HO_2 leads to disproportionation into hydrogen peroxide (H_2O_2) and O_2 (Reaction 7).[46] In the presence of both Na^+ and OH^-, which is effectively the dissolution state of sodium hydroxide (NaOH), a solid crystallite of NaOH can precipitate with a higher concentration of OH^- produced. Further reaction between NaOH and H_2O_2 from Reaction 7 leads to the formation of $Na_2O_2 \cdot 2H_2O$ *via* peroxo–hydroxylation, whose reverse reaction is well known (Reaction 8)[48]. In order to support our proposed reaction mechanism, we chose several intermediate reactions which should be verified according to the reaction model. Figure 3–15 to Figure 3–18 demonstrate that O_2^- plays an important role after the dissolution of NaO_2 in converting the discharge product to $Na_2O_2 \cdot 2H_2O$ via degradation of the electrolyte involving OH^- and H_2O_2. These identifications strongly support the proposed mechanism of competing

electrochemical and following chemical reactions in Na–O_2 batteries. The reaction equations are summarized below:

Discharge/Charge: $Na^+ + O_2 + e^- \leftrightarrow NaO_2$ (Electrochemical reaction)

Dissolution/Ionization: $NaO_2 \rightarrow Na^+ + O_2^-$

Proton abstraction: $HA + O_2^- \rightarrow A^- + HO_2$

Disproportionation: $2\ HO_2 \rightarrow H_2O_2 + O_2$

Oxidative decomposition: $A^- + HO_2 \rightarrow CO_2, H_2O, OH^-$

Peroxo–hydroxylation: $2\ Na^+ + 2\ OH^- + H_2O_2 \rightarrow Na_2O_2 \cdot 2H_2O$

To experimentally simulate Reaction 4–6 in Figure 3–15, firstly, we generated O_2^- in the electrolyte composed with 10 mM $TBAClO_4$ in DEGDME in the symmetric cell as shown in Fig. S6. The simulated coulomb was 5 mAh, which is 5–fold excess amount of electrochemically formed NaO_2 with the discharge. If we exclude the shuttle effect during the discharge, the concentration of O_2^- is approximately 0.93 M compared to the volume of injected electrolyte (200 μl).

After allowing the relaxation of O_2^- generated in Figure 3–16 in the presence of the electrolyte, the electrolyte was examined by FTIR to identify

the chemical reactions triggered by O_2^-. As compared to the as–prepared electrolyte, it was observed that the broad peak at about 3400 cm^{-1} evolves, which corresponds to νO–H stretch. This indicates the formation of free OH^- with the chemical reaction of O_2^- with the electrolyte. Furthermore, it was found that a small δO–H band and νC=O stretch arise at around 1625 cm^{-1} and 1728 cm^{-1}, respectively. The former signal also corresponds to the formation of the free OH^-, and the latter could be attributed to the trace amount of carboxylic functional groups (–COOH) in the byproduct. The presence of H_2O_2 was difficult to confirm from the FTIR due to the overlaps of signatures with DEGDME and will be discussed in Fig. S8 with iodometric experiments. The identification of νO–H, δO–H, νC=O band in the electrolyte strongly support the Reaction 6 in Figure 3–14.

To solve the uncertainties in FTIR spectra, we carried out the iodometric determinations to supplement the FTIR results above and verify the presence of H_2O_2 as shown in Figure 3–17. When the electrolyte exposed to O_2^- was added to the basis of 1 M KI aqueous solutions, which were initially transparent, the color of the solution was immediately changed to yellow. It indicates the oxidation of iodide ion (I^-) to triiodide ion (I_3^-), which was

induced by the presence of H_2O_2 *via* the reaction ($2\ I^- + 2\ H^+ + H_2O_2 \rightarrow I_3^- + 2\ H_2O$). Rest of the chemical additives such as as–prepared electrolyte or CH_3COOH do not change the color of the iodide solution. This observation supports that H_2O_2 was formed after the chemical reactions coupled with ORR, and validates Reaction 7 in Figure 3–14.

On the basis of byproducts from Reaction 6 and 7 in Figure 3–14, we attempted to simulate the formation of $Na_2O_2 \cdot 2H_2O$ as proposed in Reaction 8 ($2\ NaOH + H_2O_2 \rightarrow Na_2O_2 \cdot 2H_2O$). 0.5 M H_2O_2 aqueous solution was added dropwise to the anhydrous ethanol solution of 1 M NaOH. Because NaOH is insoluble in ether–based solvents, the solvent was used with the anhydrous ethanol to reproduce the effectively dissolved state of NaOH. After the mixing, it was found that the white precipitates were immediately formed. The retrieved precipitates were examined by XRD after drying under vacuum for 30 min. Figure 3–18 identifies that the main phase of precipitates were $Na_2O_2 \cdot 2H_2O$ with a trace amount of other phases that might be formed during the process. The formation of $Na_2O_2 \cdot 2H_2O$ strongly supports the proposed Reaction 8 in Figure 3–14.

It is noteworthy that a similar behavior has been recently reported for reactions in Li–O_2 batteries. The solvating environment was demonstrated to alter the stability of the intermediates, such as a lithium superoxide (LiO_2), thus affecting the overall reaction paths.[27, 36] LiO_2 is a precedent phase with the direct reaction of a Li cation and superoxide anion (O_2^-), which readily decomposes into lithium peroxide (Li_2O_2) *via* either an electrochemical surface reaction or disproportionation.[27, 36] Although LiO_2 is known to be unstable,[49, 50] it was recently demonstrated that LiO_2 might be dissolved into the electrolyte and aid in the formation of the toroidal Li_2O_2 *via* a solution reaction under highly solvating conditions.[27] NaO_2 shares this dissolving nature with LiO_2 even though the thermodynamic stability of NaO_2 warrants its formation as a discharge product. The significant dissolution of NaO_2 supports the conclusion that the dominant reaction in Na–O_2 batteries relies on the solution–mediated reactions of nucleation and growth of NaO_2[21, 34, 35] and implies that the capacities and morphology of the reaction products would be greatly affected by the energetics of NaO_2 under various conditions (such as different electrolytes and current rates). This is also supplemented with the recently reported

observations[21, 34] and operating mechanism[35] in terms of the various states of electrochemical and chemical reactions.

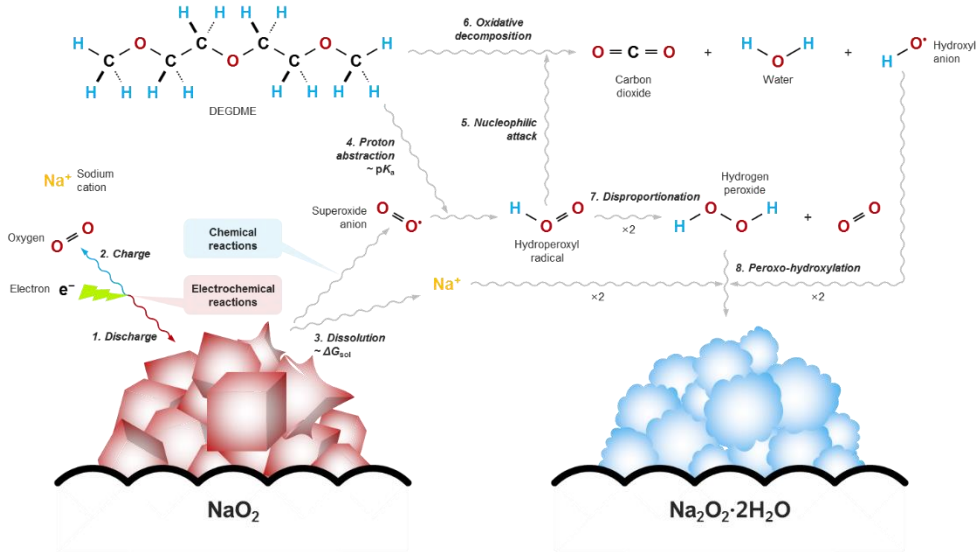

Figure 3–14. **Schematic of the proposed mechanism illustrating the electrochemical and chemical reactions under various operating conditions.** For the electrochemical reaction, NaO_2 is formed and decomposed during discharge/charge (Reaction 1, 2). For the chemical reaction, NaO_2 is dissolved and ionized into the electrolyte (Reaction 3), which promotes the undesired degradation of the electrolyte (Reaction 4–6). $Na_2O_2 \cdot 2H_2O$ is formed during the subsequent chemical reactions (Reactions 7, 8).

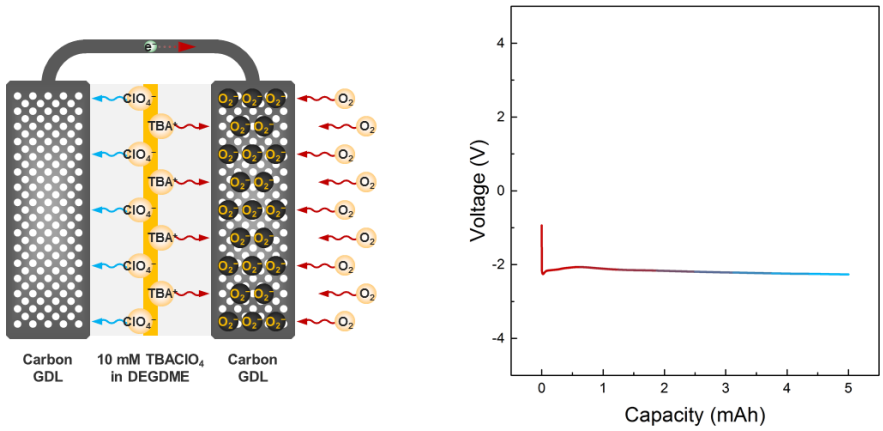

Figure 3–15. Schematic and electrochemical profile of the symmetric cell for the generation of O_2^-. Cell was consisted with GDL / glass separator / GDL. The electrolyte was 10mM $TBAClO_4$ in DEGDME. The capacity of ORR was about 5 mAh.

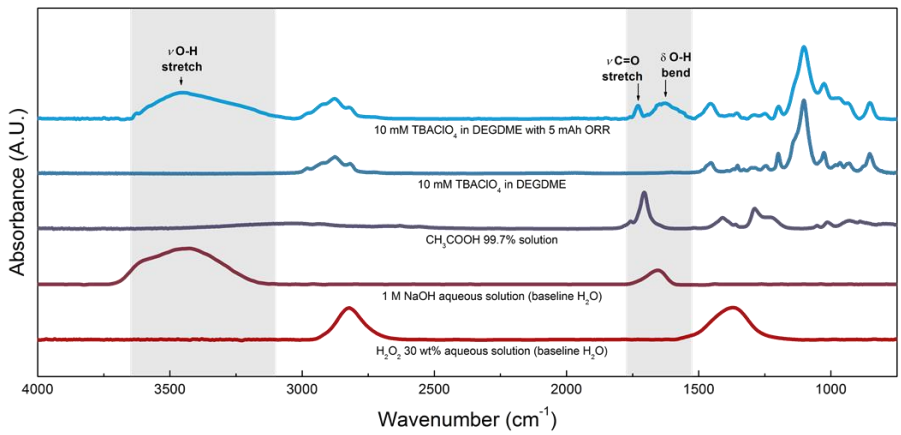

Figure 3–16. FTIR spectra with the experimentally simulated ORR. H_2O_2 30 wt% aqueous solution, 99.7 % purified CH_3COOH, 10mM of $TBAClO_4$ and 10mM of $TBAClO_4$ in DEGDME applied ORR (from bottom to top).

Figure 3–17. Iodometric titrations to check the presence of H_2O_2. (a) 1 M KI in H_2O (5 ml), (b) 1 M KI in H_2O (5 ml) adding 30 wt% H_2O_2 (200 μl), (c) 1 M KI in H_2O (5 ml) adding 10 mM $TBAClO_4$ in DEGDME (200 μl), (d) 1 M KI in H_2O (5 ml) adding 10 mM $TBAClO_4$ in DEGDME with ORR for 5 mAh (200 μl), (e) 1 M KI in H_2O (5 ml) adding 99.7 % acetic acid (200 μl)

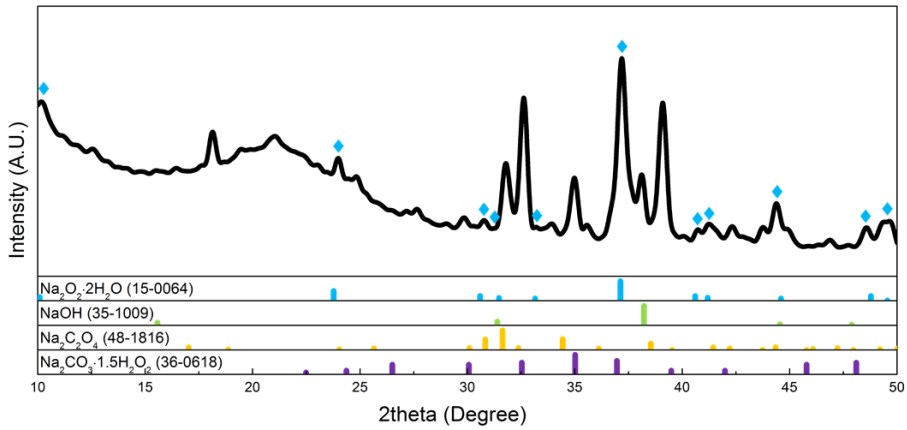

Figure 3–18. XRD analysis of chemically synthesized $Na_2O_2 \cdot H_2O$ based on the reaction equation of $2\ NaOH + H_2O_2 \rightarrow Na_2O_2 \cdot 2H_2O$.

3.4 Conclusion

We successfully demonstrated the interplay of the diverse competing reactions in Na–O_2 batteries. The time–dependent chemical reactions were identified as being triggered from the dissolution and ionization of the electrochemically formed NaO_2 in the electrolyte. The liberated O_2^- reacts with the electrolyte solvent to form $Na_2O_2 \cdot 2H_2O$ following a series of intermediate steps. The $Na_2O_2 \cdot 2H_2O$ in the air electrode requires a higher energy for the decomposition, which leads to the increased charge overpotential and irreversibility of Na–O_2 cells. This report is the first to correlate the electrochemical and chemical reactions with the operating conditions in Na–O_2 batteries, and our findings concerning the relationships among different phases resolve the conflicting observations of different discharge products in previous Na–O_2 batteries. To prepare a better performing Na–O_2 battery, a strategy to prevent the transformation of NaO_2 into $Na_2O_2 \cdot 2H_2O$ while still allowing the solution–mediate discharge reaction is necessary. We hope that the findings of this study can provide a basis for researchers to navigate and direct the reactions in Na–O_2 batteries to achieve high efficiency and rechargeability.

3.5 References

1. Tarascon, J.M. and M. Armand, *Issues and challenges facing rechargeable lithium batteries.* Nature, 2001. **414**(6861): p. 359–367.

2. Kang, K., *et al.*, *Electrodes with High Power and High Capacity for Rechargeable Lithium Batteries.* Science, 2006. **311**(5763): p. 977–980.

3. Abraham, K.M. and Z. Jiang, *A polymer electrolyte–based rechargeable lithium/oxygen battery.* Journal of the Electrochemical Society, 1996. **143**(1): p. 1–5.

4. Bruce, P.G., *et al.*, *Li–O_2 and Li–S batteries with high energy storage.* Nature Materials, 2012. **11**(1): p. 19–29.

5. Lim, H.–D., *et al.*, *Superior Rechargeability and Efficiency of Lithium–Oxygen Batteries: Hierarchical Air Electrode Architecture Combined with a Soluble Catalyst.* Angewandte Chemie–International Edition, 2014. **126**(15): p. 4007–4012.

6. Peng, Z., *et al.*, *A Reversible and Higher–Rate Li–O_2 Battery.* Science, 2012. **337**(6094): p. 563–566.

7. Ottakam Thotiyl, M.M., *et al.*, *A stable cathode for the aprotic Li–O_2 battery.* Nature Materials, 2013. **12**(11): p. 1050–1056.

8. Débart, A., *et al.*, *α–MnO_2 Nanowires: A Catalyst for the O_2 Electrode in Rechargeable Lithium Batteries.* Angewandte Chemie–International Edition, 2008. **47**(24): p. 4521–4524.

9. Freunberger, S.A., *et al.*, *The lithium–oxygen battery with ether–based electrolytes.* Angewandte Chemie – International Edition, 2011. **50**(37): p. 8609–8613.

10. Yabuuchi, N., *et al.*, *Research Development on Sodium–Ion Batteries.* Chemical Reviews, 2014. **114**(23): p. 11636–11682.

11. Hartmann, P., *et al.*, *A rechargeable room–temperature sodium superoxide (NaO_2) battery.* Nature Materials, 2012. **12**(3): p. 228–232.

12. Bender, C.L., *et al.*, *On the Thermodynamics, the Role of the Carbon Cathode, and the Cycle Life of the Sodium Superoxide (NaO_2) Battery.* Advanced Energy Materials, 2014. **4**(12): p. 1301863.

13. McCloskey, B.D., J.M. Garcia, and A.C. Luntz, *Chemical and Electrochemical Differences in Nonaqueous Li–O_2 and Na–O_2 Batteries.* The Journal of Physical Chemistry Letters, 2014. **5**(7): p. 1230–1235.

14. Hartmann, P., *et al.*, *Pressure Dynamics in Metal–Oxygen (Metal–Air) Batteries: A Case Study on Sodium Superoxide Cells.* The Journal of Physical Chemistry C, 2014. **118**(3): p. 1461–1471.

15. Liu, W., *et al.*, *An enhanced electrochemical performance of a sodium–air battery with graphene nanosheets as air electrode catalysts.* Chemical Communications, 2013. **49**(19): p. 1951–1953.

16. Li, Y., *et al.*, *Superior catalytic activity of nitrogen–doped graphene cathodes for high energy capacity sodium–air batteries.* Chemical Communications, 2013. **49**(100): p. 11731–11733.

17. Hu, Y., *et al.*, *Porous perovskite calcium–manganese oxide microspheres as an efficient catalyst for rechargeable sodium–oxygen batteries.* Journal of Materials Chemistry A, 2015. **3**(7): p. 3320–3324.

18. Kim, J., *et al.*, *Sodium–oxygen batteries with alkyl–carbonate and ether based electrolytes.* Physical Chemistry Chemical Physics, 2013. **15**(10): p. 3623–3629.

19. Yadegari, H., *et al.*, *On rechargeability and reaction kinetics of sodium–air batteries.* Energy & Environmental Science, 2014. **7**(11): p. 3747–3757.

20. Zhao, N., C. Li, and X. Guo, *Long–life Na–O_2 batteries with high energy efficiency enabled by electrochemically splitting NaO_2 at a low overpotential.* Physical Chemistry Chemical Physics, 2014. **16**(29): p. 15646–15652.

21. Ortiz–Vitoriano, N., *et al.*, *Rate–Dependent Nucleation and Growth of NaO_2 in Na–O_2 Batteries.* The Journal of Physical Chemistry Letters, 2015. **6**(13): p. 2636–2643.

22. Fishman, M., *et al.*, *Accuracy of exchange–correlation functionals and effect of solvation on the surface energy of copper.* Physical Review B, 2013. **87**(24): p. 245402.

23. Mathew, K., *et al.*, *Implicit solvation model for density–functional study of nanocrystal surfaces and reaction pathways.* The Journal of Chemical Physics, 2014. **140**(8): p. 084106.

24. Burgess, J., *Metal ions in Solution.* Chichester: Horwood Ellis: New York, 1978.

25. Ben–Amotz, D., F.O. Raineri, and G. Stell, *Solvation Thermodynamics: Theory and Applications.* Journal of Physical Chemistry B, 2005. **109**(14): p. 6866–6878.

26. Yadegari, H., *et al.*, *Three–Dimensional Nanostructured Air Electrode for Sodium–Oxygen Batteries: A Mechanism Study toward the Cyclability of the Cell.* Chemistry of Materials, 2015. **27**(8): p. 3040–3047.

27. Aetukuri, N.B., *et al.*, *Solvating additives drive solution–mediated electrochemistry and enhance toroid growth in non–aqueous Li–O_2 batteries.* Nature Chemistry, 2015. **7**(1): p. 50–56.

28. Schroeder, M.A., *et al.*, *DMSO–Li_2O_2 Interface in the Rechargeable Li–O_2 Battery Cathode: Theoretical and Experimental Perspectives on Stability.* ACS Applied Materials & Interfaces, 2015. **7**(21): p. 11402–11411.

29. Kumar, N., *et al.*, *Surface–Mediated Solvent Decomposition in Li–Air Batteries: Impact of Peroxide and Superoxide Surface Terminations.* The Journal of Physical Chemistry C, 2015. **119**(17): p. 9050–9060.

30. Kwabi, D.G., *et al.*, *Chemical Instability of Dimethyl Sulfoxide in Lithium–Air Batteries.* The Journal of Physical Chemistry Letters, 2014. **5**(16): p. 2850–2856.

31. Wang, Q., X.–Q. Yang, and D. Qu, *In situ ESR spectro–electrochemical investigation of the superoxide anion radical during the electrochemical O_2 reduction reaction in aprotic electrolyte.* Carbon, 2013. **61**(0): p. 336–341.

32. Eastland, G.W. and M.C. Symons, *Electron spin resonance studies of superoxide ions produced by radiolysis in alcoholic media.* The Journal of Physical Chemistry, 1977. **81**(15): p. 1502–1504.

33. Schechter, D.L. and J. Kleinberg, *Reactions of Some Metal Salts with Alkali Superoxides in Liquid Ammonia.* Journal of the American Chemical Society, 1954. **76**(12): p. 3297–3300.

34. Hartmann, P., *et al.*, *Discharge and Charge Reaction Paths in Sodium–Oxygen Batteries: Does NaO_2 Form by Direct Electrochemical Growth or by Precipitation from Solution?* The Journal of Physical Chemistry C, 2015. **119**(40): p. 22778–22786.

35. Xia, C., *et al.*, *The critical role of phase–transfer catalysis in aprotic sodium–oxygen batteries.* Nature Chemistry, 2015. **7**(6): p. 496–501.

36. Johnson, L., *et al.*, *The role of LiO_2 solubility in O_2 reduction in aprotic solvents and its consequences for Li–O_2 batteries.* Nature Chemistry, 2014. **6**(12): p. 1091–1099.

37. Hall, P. and B. Selinger, *Better estimates of exponential decay parameters.* The Journal of Physical Chemistry, 1981. **85**(20): p. 2941–2946.

38. Maricle, D.L. and W.G. Hodgson, *Reducion of Oxygen to Superoxide Anion in Aprotic Solvents.* Analytical Chemistry, 1965. **37**(12): p. 1562–1565.

39. Okoshi, M., *et al.*, *Theoretical Analysis on De–Solvation of Lithium, Sodium, and Magnesium Cations to Organic Electrolyte Solvents.* Journal of the Electrochemical Society, 2013. **160**(11): p. A2160–A2165.

40. Ziegler, M. and J. Madura, *Solvation of Metal Cations in Non–aqueous Liquids.* Journal of Solution Chemistry, 2011. **40**(8): p. 1383–1398.

41. Petrowsky, M.A., *Ion transport in liquid electrolytes*, in *Department of Chemistry and Biochemistry*2008, University of Oklahoma: Norman, OK.

42. Kashchiev, D. and G. Van Rosmalen, *Review: nucleation in solutions revisited.* Crystal Research and Technology, 2003. **38**(7-8): p. 555–574.

43. Takiyama, H., *Supersaturation operation for quality control of crystalline particles in solution crystallization.* Advanced Powder Technology, 2012. **23**(3): p. 273–278.

44. Khetan, A., A. Luntz, and V. Viswanathan, *Trade–Offs in Capacity and Rechargeability in Nonaqueous Li–O_2 Batteries: Solution–Driven Growth versus Nucleophilic Stability.* The Journal of Physical Chemistry Letters, 2015. **6**(7): p. 1254–1259.

45. Khetan, A., H. Pitsch, and V. Viswanathan, *Solvent Degradation in Nonaqueous Li–O_2 Batteries: Oxidative Stability versus H–Abstraction.* The Journal of Physical Chemistry Letters, 2014. **5**(14): p. 2419–2424.

46. Sawyer, D.T. and J.S. Valentine, *How super is superoxide?* Accounts of Chemical Research, 1981. **14**(12): p. 393–400.

47. Freunberger, S.A., *et al.*, *The Lithium–Oxygen Battery with Ether–Based Electrolytes.* Angewandte Chemie–International Edition, 2011. **50**(37): p. 8609–8613.

48. Hill, G.S., *et al.*, *The X–ray structure of a sodium peroxide hydrate, $Na_2O_2 \cdot 8H_2O$, and its reactions with carbon dioxide: relevance to the brightening of mechanical pulps.* Canadian Journal of Chemistry, 1997. **75**(1): p. 46–51.

49. Zhai, D., *et al.*, *Interfacial Effects on Lithium Superoxide Disproportionation in Li–O_2 Batteries.* Nano Letters, 2015. **15**(2): p. 1041–1046.

50. Zhai, D., *et al.*, *Raman Evidence for Late Stage Disproportionation in a Li–O_2 Battery.* The Journal of Physical Chemistry Letters, 2014. **5**(15): p. 2705–2710.

Chapter 4. Summary

By summarizing the findings, it is quite important to suppress the chemical reactions, in order to enhance the feasibility of Na–O_2 batteries. To maintain the reversible redox reactions, the dissolution issues of NaO_2 must be carefully arranged to avoid the formation of unwanted $Na_2O_2 \cdot 2H_2O$. The investigated kinetics of chemical reactions in this work can be altered with the other experimental conditions such as a types of carbon (surface area, terminating heteroatom), electrolyte solvent (donor number, dielectric constant), electrolyte salt (concentration, anion group), and thermodynamic criteria (temperature, O_2 partial pressure). Therefore in Na–O_2 batteries, it should be understood the fundamental behaviors and mechanisms, then found the optimum point which shows the superior characteristics among those variables. We expect this discussion can give some valuable navigates for the researchers to adjust the directions of net reaction in the metal–air batteries.

Chapter 5. Abstract in Korean

최근 높은 에너지밀도를 가진 에너지저장장치에 대한 수요증가로 인해, 고용량의 특성을 지니는 메탈–에어 배터리가 활발히 연구되고 있다. 이중에서 소듐–에어 배터리는 리튬–에어 배터리에 비해 값싸고 흔한 원료 구성 및 낮은 충전 과전압으로 인해 매력적인 차세대 메탈–에어 배터리로 각광받고 있다. 하지만 서로 상반되는 방전산화물의 학계 보고와 그에 따른 특성 변화는 소듐–에어 배터리의 반응 메커니즘에 대한 이해를 저해하고 있다.

먼저 Chapter 2 에서는, 탄산염계 전해질과 비탄산염계 전해질을 이용한 소듐–에어 배터리를 연구하였다. 두 가지 종류의 전해질 모두 리튬–에어 배터리에 준하는 높은 방전용량이 발현되는 것을 확인할 수 있었지만, 리튬 대비 소듐의 0.3 V 낮은 표준 산화환원 전위 차이로 인해서 방전 전압 또한 그만큼 낮아지는 것을 확인하였다. 두 가지 전해질을 사용한 조건에서 각각 서로 다른 방전산화물이 생성되는 것을 분석하였고, 이에 대해 예상되는 반응 메커니즘을 제안하고 리튬–에어 배터리와 비교하였다.

Chapter 3 에서는, 소듐-에어 배터리에서 전기화학 반응과 화학 반응의 경쟁으로 인해 NaO_2 가 용해 및 이온화되어 O_2^-를 방출하여 $Na_2O_2 \cdot 2H_2O$ 가 생성되는 것을 규명하였다. 방전산화물이 NaO_2 가 아닌 경우엔, 충전 과전압이 급격히 증가하는 것을 확인하였다. 이 보고는 이종 방전산화물의 생성 원인과 규명하고 상반되는 충전 과전압과의 연관성을 밝힌 첫번째 보고로서, 여기서 제안한 메커니즘 모델은 소듐-에어 배터리 내부에서 일어나는 반응들을 이해하여 제어하여 높은 충방전 효율과 성능을 달성하는데 통찰력을 제공할 것으로 예상된다.